

Ru@30400

INSTITUTE FOR HIGH ENERGY PHYSICS

IHEP-OEF--90-81

И О Б Э 90-81

030

(IIVE-OEF--90-81)

EXPERIMENTS ON HYPERON BEAM OF UNK
Collaboration IHEP-ITEP-LINF-INPS MSU

Protvino 1990

Abstract

Garkusha V.I. et al. Experiments on Hyperon Beam of UNK (Collaboration IHEP-ITEP-LINP-INPS MSU): IHEP Preprint 90-81. - Protvino, 1990. - p. 87, figs. 28, tables 17, refs.: 42.

The experimental program for the UNK hyperon beam is considered. It is expected, that a focused "pure" Σ hyperon beam with $P \approx 2700$ GeV/c, intensity $> 10^7$ Σ^- /s and $> 85\%$ of Σ^- hyperons may be created in this machine. The magnetized iron shielding will allow one to reduce the muon "halo" by 2 orders of magnitude. The experiments on the study of strange-charmed and strange-beauty baryons, search for exotic states with strangeness and charm and cryptoexotic strange hadrons with hidden charm and beauty are discussed. The possibilities of the hyperon beam for these processes are unique. Future studies of hyperon form-factors and structure functions of the processes in the nuclear Coulomb field, rare decays of charmed and beauty particles, τ -leptons and hyperons are also considered.

Аннотация

Гаркуша В.И. и др. Исследование на гиперонном пучке УНК (Сотрудничество ИЯЭ-ИТЭФ-ЛНП-ИЯФ МГУ): Препринт ИЯЭ 90-81. - Протвино, 1990. - 87 с., 28 рис., 17 табл., Сибмогр.: 42.

Рассмотрена программа экспериментов на гиперонных пучках УНК. Ожидается, что на этом ускорителе может быть создан фокусированный "чистый" пучок Σ^- -гиперонов с импульсом ≈ 2700 ГэВ/с, с интенсивностью $> 10^7$ Σ^- /сек, с содержанием Σ^- -гиперонов $> 85\%$. Мюнное "гало" будет снижено на 2 порядка с помощью намагнитченной железной защиты. Обсуждаются эксперименты по исследованию странно-очарованных и странно-прекрасных барионов, поиски экзотических состояний со скрытым чармом или прелестью. Возможности гиперонного пучка для этих процессов являются уникальными. Рассмотрены также перспективы исследования форм-факторов и структурных функций гиперонов, процессов в кулоновском поле ядер, редких распадов очарованных и прекрасных частиц, τ -лептонов и гиперонов.

INSTITUTE FOR HIGH ENERGY PHYSICS

И Ф Б Э 90-81

090

EXPERIMENTS ON HYPERON BEAM OF UNK
Collaboration IHEP-ITEP-LINP-INPS MSU*)

Protvino 1990

*) Members of collaboration

V.I.Garkusha, S.V.Golovkin, A.M.Gorin, A.A.Derevshchikov,
V.A.Dorofeev, A.A.Kozhevnikov, A.S.Konstantinov,
V.I.Kotov, V.P.Kubarovsky, N.Yu.Kul'man, A.I.Kulyavtzev,
I.A.Kurochkin, V.P.Kurshetsov, A.E.Kushnirenko,
L.G.Landsberg, V.V.Molchanov, V.I.Mukhin, P.N.Novoseltzev,
A.V.Skleznev, V.I.Solyanik, A.V.Uzunyan,
V.I.Viktorov, O.D.Tzay, A.A.Zaitzhenko

IHEP

B.M.Abramov, I.M.Belyaev, S.A.Bulychev, Yu.L.Griashkin,
V.S.Kaftanov, Yu.V.Korchagin, V.V.Kulikov, A.A.Lebedev,
G.S.Lomkatzi, A.F.Nilov, O.I.Pogorelko, S.V.Proshin,
I.A.Radkevich, V.T.Smolyankin, N.Tkach

IYEF

V.B.Borkovski, Yu.L.Dokschitzer, V.T.Grachev,
A.P.Kashuk, A.B.Khanzadiev, V.A.Khoze, G.A.Kolomenski,
G.Z.Obrandt, V.M.Samsonov, V.V.Sarantzev,
V.A.Shagel'ski, A.I.Smirmov, N.N.Smirmov, A.B.Sokornov,
V.M.Suvorov, N.K.Terent'ev, N.G.Ural'tzev, A.A.Vorob'ev

LINP

N.N.Balamatov, E.A.Chudakov, R.K.Dement'ev,
I.S.Pilimonov, E.M.Leikin, I.V.Nadezhdin,
A.V.Nemetkin, Yu.V.Nimsen, N.P.Novokshanov,
V.I.Rud', L.M.Sheglova, A.N.Solemin,
B.A.Yur'ev, N.P.Zotov

INPS MSU

It is a preliminary list of participants which will be clarified in the course of constructing the facility. Besides possibilities to extend collaboration are being discussed.

I. INTRODUCTION

A very high primary energy of the UNK proton beam allows one to produce high quality intense hyperon beam, whose characteristics are very close to those of a usual hadron beams. At the UNK energies the decay length for charged hyperons is about 50-100 m. Moreover in this case it becomes possible to form a focused hyperon beam in the beam channel with magnetic optics, as well as to construct a very reliable shielding, designed for the operation with the ultimate intensity of the proton beam (up to $3 \cdot 10^{14}$ ppc). The shielding includes an active guard system of magnetized iron slabs, which greatly reduces the muon background in the setup area. All these measures taken together make it possible to realize the operational modes in the range of $x_p > 0.9$, where $I(\Sigma^-) \gg I(\Sigma^+)$, which will be done for the first time in experiments. Almost a pure Σ^- beam with momentum of $P_\Sigma = 2.7$ TeV/c and intensity $> 10^7 \Sigma^- \cdot s^{-1}$ may be obtained at the UNK 3 TeV machine. These properties of the UNK hyperon beam are unique.

The main trends in the research program on the UNK hyperon beam are connected with the problems, for the study of which the increase of the hyperon initial energy and high quality of the hyperon beam are of utmost importance. These problems are as follows:

1. The spectroscopy of heavy strange-charmed and strange-beauty baryons, measurement of the life time and investigation of their weak decays. Hyperon beam experiments are greatly advantageous in this case as compared with other experiments as far as the baryon production cross sections and background con-

ditions are concerned. It is also worth stressing here that the hyperon beam is the most effective source for fragmentational B_s^- and B_s^0 mesons.

2. Study of $B_s^0 \rightarrow \bar{B}_s^0$ oscillations and search for rare decays of B-mesons.

3. Search for heavy exotic and cryptoexotic baryonic and mesonic states with strange and charmed (beauty) quarks.

4. Study of rare weak decays of hyperons. The sensitivity in these experiments will be 10^{-13} for the decays Σ^- , 10^{-11} for the decays Ξ^- and Λ , and 10^{-8} for the σ^- decays.

5. Study of the small cross section processes, for which high energy and intensity of the UNK hyperon beam turns out to be essential: muon pair production, investigation of the hyperon structure functions and comparison with the corresponding processes for nucleons; investigation of the Σ^- hyperon scattering on electrons and measurement of elastic and transition formfactors for Σ^- hyperons and $\Sigma^- \Sigma^*$ vertex; Y^* hyperon resonance production in the nucleus Coulomb field.

6. A standard investigation program for hyperon strong interactions but in a new energy region (total cross section measurements, study of elastic scattering, exclusive and inclusive processes, polarization experiments with hyperons, etc.).

All the experiments at the UNK mentioned above have considerable advantages as compared with the experiments at the TEVATRON, they are much higher energy and (or) higher quality of the hyperon beam.

It is also assumed that some measurements will be carried out in other beams which can be extracted with the aid of the hyperon magnetic channel onto the target of the experimental facility (π meson beam, proton beam). Such experiments, providing very close conditions, allow one to compare the data on the production of heavy particles and muon pairs with large masses by different primary hadrons with minimal systematic errors; to compare their structure functions, formfactors and other characteristics. Besides the intense proton beam (10^{11} - 10^{12} pps) in the underground hall of the hyperon area will make it possible to carry out special experiments on the study of rare well identified decays of heavy particles (e.g., two particle decays

of B mesons). Precise measurement technique for the tracks to have a very good mass resolution may be applied here. These experiments may play an important role in the search of CP-invariance nonconservation effects in B decays, or forbidden decays with leptonic number nonconservation (B^0 , $D^0 \rightarrow \mu e$, $\tau \rightarrow 3\mu$, etc.) or the decays caused by FCNC interactions (B^0 , $D^0 \rightarrow \mu^+ \mu^-$). The main trends in the proposed program were discussed by us many times in a number of the reports at the Workshops on the UNK experimental program, at the XXXII Session of the Scientific-Coordinating Council of IHEP and other meetings (see, e.g., [1]).

The leading role in this program seems to belong to the experiments on heavy quark physics, which will enable a decisive check of the standard model, the study of hadron structure and of the properties of exotic states with beauties, charmed and strange quarks. Besides we will be able to carry out a search for low energy manifestations of new fundamental interactions. Many of these possibilities are unique. Let us now proceed to a detailed presentation of some aspects of the project and to consideration of peculiarities of some experiments in the UNK hyperon beam.

2. UNK HYPERON BEAM [2]

The scheme of the UNK hyperon beam, which includes a system of particle quadrupole focusing and active muon shielding, is presented in Fig.1. The first set of four radiation-resistant magnets M1-M4 with an aperture layed with tungsten, allows to separate the formed Σ^- hyperon beam from the proton beam which did not interact in the target. The latter one is dumped then in a special absorber, installed right after the first set of the magnets. Depending on the operational mode the space resolution of the secondary particle beam and of the proton beam on the front edge of the absorber is 30-40 mm. The second set of the magnets M5-M8 makes the bending angle of the hyperon beam 4.8 mrad, which enables further purification of the formed Σ^- hyperon beam. The collimator G2 determined the angle of capturing the secondary particles into the beam channel. A

doublet of SC quadrupole lenses Q1-Q6 realizes the focusing of the beam onto the target of the experimental facility. And the last set of two magnets M9 and M10 together with the collimator C3 provides the purification of the formed Σ^- hyperon beam removing neutrons and π^- mesons, produced in the Σ^- hyperon decay in the beam straightline section. The main parameters of the hyperon beam are presented in Table 1.

Table I. The Main Parameters of the Hyperon Beam.

Beam line length	100m
Total deflection angle	9.6 mrad
for M1-M8 set including	4.8 mrad
Maximum momentum	3000 GeV/c
Horizontal angular acceptance	0.3 mrad
Vertical angular acceptance	0.7 mrad
Selected momentum bins (PWHM)	20 %

Secondary particle fluxes at the end of the hyperon beam channel were calculated with the data borrowed from ref.[3]. They are presented in fig.2 and Tables II and III.

Table II. Σ^- -hyperon beam characteristics.

P_0 , GeV/c	$\langle p_{\Sigma^-} \rangle$, GeV/c	σ_{p^*} , %	σ_{Σ^-} , mm	σ_{Σ^+} , mm	Σ^- hyperon intensity per incident proton	π^-/Σ^- intensity ratios
2100	2062	6.7	4.1	2.5	$5.0 \cdot 10^{-5}$	3.3
2400	2347	6.4	3.9	2.4	$4.1 \cdot 10^{-5}$	1.2
2700	2608	5.9	3.3	2.4	$2.5 \cdot 10^{-5}$	0.32
2850	2706	4.9	2.2	2.6	$1.6 \cdot 10^{-5}$	0.14
3000	2789	3.9	1.4	2.7	$8.0 \cdot 10^{-6}$	0.056

Note: Here p_0 -momentum, corresponding to the optical beam axis, $\langle p_{\Sigma^-} \rangle$ average momentum of Σ^- beam at the end of the beam line.

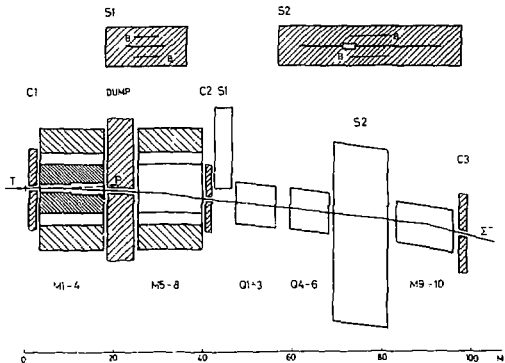


Fig. 1. Hyperon beam layout: T - target; M1-M4 - radiation resistant magnets; M5-M8 - magnets; M9, M10 - superconducting magnets; Q1-Q6 - SC quadrupole lenses; C1-C3 - collimators; DUMP - absorber to dump protons not interacting in the target; S1, S2 - magnet spoilers.

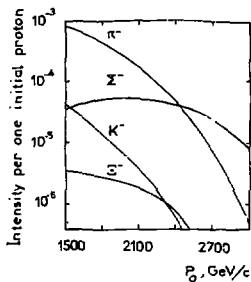


Fig. 2. Secondary particle flux at the end of the hyperon beam (for Be target 500 mm thick).

As is seen, at $x \geq 0.9$ and the intensity of the incident proton beam onto the target 10^{12} pps one may obtain almost pure Σ^- hyperon beam with intensity of 10^7 pps. Neutron and π^- meson background from the Σ^- hyperon decay is 12 and 4%, respectively.

The calculations made with the MARS10 program show that soft hadronic background from the cascade processes in the collimator is not more than 5% from the Σ^- hyperon beam intensity. Since the collimator C3 is the main source of this background, its basic parameters (length, aperture, material) should thoroughly be optimized.

To measure particle momentum in the formed beam one may use a spectrometer based on the magnets M9, M10. Putting three detectors for particle coordinate measurements in the horizontal plane downstream of the quadrupole lenses and up and downstream the magnets, one can get the momentum resolution $\sigma_p = 1\%$ with the detector resolution spatial $\sigma_x = 0.15 \text{ mm}^*$.

The scheme of the hyperon beam channel was worked out with employment of the magnet elements, assigned for other UNK beam channels. The main parameters of the magnet elements used in the hyperon beam, are presented in Table IV.

Table III. Flux of Hyperons of different types at the beam line end.

$\langle p \rangle$, GeV/c	x	$N(\Sigma^-)$, s^{-1}	$N(\Sigma^+)$, s^{-1}	$N(\Xi^-)$, s^{-1}	$N(n^-)$, s^{-1}
2700	0.90	$\sim 10^7$	~ 10	$3 \cdot 10^4$	$3 \cdot 10$
2250	0.75	$4 \cdot 10^6$	$\sim 10^2$	$1 \cdot 10^5$	$1.4 \cdot 10^2$
1500	0.50	$4 \cdot 10^5$	$1.5 \cdot 10^2$	$3.5 \cdot 10^4$	$3 \cdot 10$

Note: Hyperon intensity is given under condition, that total number of particles in the beam $\sim 10^7$ pps; $x = \langle p \rangle / 3 \text{ TeV/c}$.

*) Rodoscopes with scintillating fiber may be used for this purpose (see Chapter V).

Table IV. The Basic Magnetic Elements Used in the Hyperon Beam Channel.

Equipment unit	Max. field (Kgauss); field gradient (Kgauss)	Length in iron (m)	Transverse dimensions in iron (cm)	Aperture (cm)
Bending magnet				
radiation resistive	20	3.0	120*74	30*4
Bending magnet	20	3.0	120*74	30*4
SC bending magnet	40	6.0	ø 40	ø 7
sc quadrupole lens	9	3.0	ø 40	ø 7

The decay of π , K mesons from hadronic cascades produced in the target and beam channel elements is the main muon source in the hyperon beam channel. The forming of the muonic field is practically accomplished at the exit of the main set of magnet M1-M8, considerable influence on its characteristics being exercised by the magnetic field not only in the magnet gap but in their yokes.

The integral muon flux onto the experimental area is equal to $3.0 \cdot 10^{-5}$ μ /proton, which is 1+2 times higher than the π^- hyperon beam intensity.

As it follows from the calculations and estimates [2] an efficient and compact active shielding against muons in the hyperon beam channel may be provided if muons are deflected vertically. Magnetic spoilers with flat current, whose transverse horizontal field with the magnetic inductance of about 1.5 Tl, are to be used for this purpose.

An optimized system of two magnetic spoilers with oppositely directed currents (fig.1) reduces the integral muonic flux onto the experimental area 85 times and thus lowering the relative muon background N_{μ}/N_{Σ} down to <3%. The first spoiler $0.6 \times 0.4 \times 4 \text{ m}^3$ suppresses the source of positive background muons, deflecting them from the middle beam channel plane, the second spoiler $1.6 \times 0.4 \times 12 \text{ m}^3$, suppresses the source of negative background muons. The distance of 30 m between the spoiler centres turns out to be sufficient to avoid the capturing of the positive muons deflected by the first spoiler, in the second one.

3. EXPERIMENTAL FACILITY FOR HYPERON INVESTIGATIONS

3.1. General structure of the setup

The experimental facility for the investigations to be carried out in the UNK hyperon beam should be multipurpose so as to be capable to deal with a wide program spoken about in the Introduction. All these impose quite stringent and sometimes even contradictory requirements on its characteristics. The setup should have large acceptance which would allow for the detection of heavy particle production in the region of $0 < X_F < 1$ including processes of associative production, which is very important for tagging B^0 - and D^0 -mesons with definite heavy quark flavors. The accuracy of measuring the angles and momenta should be such as to provide the selection of processes with very small momentum transfer ($|t| < 0.001 \text{ (GeV/c)}^2$) which is necessary for the investigation of the reactions in the nucleus Coulomb field. Simultaneous detection and reliable identification of both charged and neutral secondaries (e.g., $\pi^0 \rightarrow 2\gamma$; $\eta \rightarrow 2\gamma$; $\Lambda \rightarrow p\pi^-$, $K_S^0 \rightarrow \pi^+\pi^-$, etc.) are required. Ultimate accuracy for the effective mass measurements is important for the identification of heavy flavor hadronic decay channels. To study leptonic and semileptonic decays of heavy quarks we are to detect electrons and muons. The facility should also include a sophisticated vertex detector to single out the cascade decays of short-lived particles and to investigate the $B^0 \leftrightarrow \bar{B}^0$ or $D^0 \leftrightarrow \bar{D}^0$ oscillations. The vertex detector will also be used to produce triggering signals to select the events with beauty and charmed particles. In this case one should solve the problems connected with the acquisition and processing of a large amount of information and with a reliable selection of rare processes. In some cases when choosing the sizes of the setup one should foresee its capability to identify secondary hyperons decays, which may have very large decay paths (e.g., for Λ -hyperons with the momentum 1.5 TeV/c the decay length is 106 m).

As has already been noted, some of these requirements are quite contradictory. Therefore it is of vital importance that the setup should consist of modules and be easily recombined for the study of different problems. In particular, for a number of experiments the facility may greatly be simplified.

The general layout of the experimental setup for the investigations in the UNK hyperon beam is presented in fig.3. The setup consists of the following main elements:

1. hyperon beam identification system;
2. active target and vertex detector;
3. vertex magnetic spectrometer M1 to detect secondaries with intermediate momenta (with minidrift chambers and scintillation hodoscopes);
4. magnetic spectrometer M2 to detect fast secondaries (with track detectors and hodoscopes);
5. magnetic spectrometer M3 for the experiments in the region of large x_p ;
6. differential multichannel gas Cerenkov RICH counters of three types for secondary π , K, p identification in the momentum range of 3.5-35 GeV; 20-100 GeV; 50-240 GeV;
7. transition radiation detectors (TRD) for K, p identification at momenta >150 GeV/c and to single out electrons;
8. system of drift tubes and chambers for Λ decay detection;
9. hodoscope electromagnet calorimeters for photon detection;
10. hadron scintillation calorimeters;
11. muon detector;
12. front-end electronics, a system to produce a preliminary trigger, data acquisition system and processors to work out high level triggering signals;
13. computers for on-line analysis.

Table V presents the sizes of different detectors and the number of channels in the facility. These parameters were determined when simulating some characteristic processes, connected with the production and decays of particles with heavy quarks.

3.2. Simulation of the production and decay processes for baryons with heavy quarks

The RSIMUL program, which could simulate particle production, their decays, particle flight through the spectrometer with an account of multiple scattering, reconstruct particle trajectory, vertex coordinates and effective masses, was used for preliminary calculations of the facility characteristics. To choose the geometrical parameters for the setup to be used in

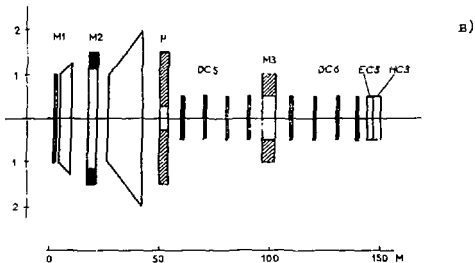
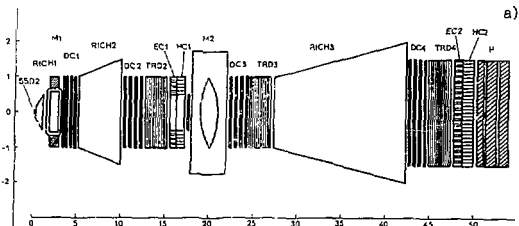


Fig. 3. Experimental facility for hyperon studies. a) Spectrometer for beauty and charmed hadron detection. b) General layout of the facility: SSD - microstrip detector; RICH1-3 - differential Cerenkov spectrometers; DC1-DC6 - minidrift chambers; TRD1-TRD4 - transition radiation detectors; M1-M3 - magnets; EC1-EC3 - electromagnetic calorimeters; MC1-MC3 - hadron calorimeters; μ - muon detector.

Table V. Characteristics of Main Detectors in the Facility

		Dimensions x (cm)	y (cm)	Step (cm)	Number of planes	Number of channels
1. Beam microstrip detector	SSP-1				6	1536
2. Vertex detector	SSD-2	1.5-4.5	1.5- -4.5	0.0025	48	30000 (20000)
3. Drift; chambers	DC1	200	100	0.4	32	12000
	DC2	200	150	0.8	32	7000
	DC3	200	150	0.9	32	7000
	DC4	300	200	0.8-1.0	32	10000-8000
					Total	35000
4. Electromagnetic calorimeters	EC1	220	180	5*5		1200
	EC2	300	200	5*5 (10*10)		2400 (1800)
					Total	3600
5. Hadron calorim- eters	HC1	220	180	10*10		300
	HC2	300	200	10*10		600
					Total	900
6. Cherenkov ring image detectors	RICH1					1000
	RICH2					5000
	RICH3					5000
7. Transition ra- diation de- tectors	TRD1	2	2	0.050	20 modules	1600
	TRD2	200	150	0.3	5 modules	6000
	TRD3	200	150	0.3	5 modules	6000
	TRD4	300	200	0.3	10 modules	17000
					Total	30800

the study of baryon spectroscopy and heavy particle physics we took, as a typical example, inclusive production of strange-beauty baryons

$$\Sigma^- + K^- \rightarrow \Sigma_b^- + X$$

for which the following cross section dependence takes place

$$Ed^3\sigma/dp^3 = \text{const} \exp(-\beta p_T^2) (1 - x_p)^n. \quad (1)$$

Here p_T is the transverse momentum, $\beta=0.15$ (GeV/c)² (so that $\sqrt{\langle p^2 \rangle} = 2.5$ GeV/c, in accordance with QCD calculations at $p_T < 4$ GeV/c).

In some part of calculations we took into account associative production of heavy particles. It was done as follows:

a) associative B-meson production was generated so that the distribution of the total transverse momentum of b particles had the form $\exp(-ap_T^2)$, where $a=0.3$ (GeV/c) 2 , and the distribution of the rapidity differences for two B particles was Gaussian with the dispersion equal to 1;

b) in the event under investigation other associative particles were produced in order to calculate the particle density in the detectors. For this purpose we simulated the production of secondary particles by pions with momentum equal to the difference of the primary beam particle momentum and that of two B particles, JETSET (Lund) program being used in this simulation.

Associative production of beauty particles was also modeled with the help of the ISAJET program.

The Σ_b baryon decays were generated in accordance with the phase volume, in this three nonleptonic decay channels convenient for detection, were considered. Their relative decay probabilities were estimated in accordance with [4] (see Table VI)

Decay (2) and (4) contain strange hyperons with mean life $(1.5-2.5) \cdot 10^{-10}$ sec. Their decay paths are presented in fig.4 with account of the relativistic factors.

Decay (4) goes on with the production of charmed baryon $S_c^+(2560)$, a "symmetric" partner of Σ_c^+ . The value for the mass splitting of these two states is not known at present. At the chosen value of the mass splitting the dominating one is the $S_c^+(2560) \rightarrow \Sigma_c^+(2460) + \gamma$ radiative decay.

Since the Σ^- trajectory may be reconstructed, all the secondary particles will be related to the corresponding decay vertices for Σ_b^- and Σ_c^+ . The possibility to detect the decay channels of beauty and charmed particles with the neutral particle emission is not so obvious since one has to determine here what vertex the neutral particle belongs to. In this case everything will be determined by the combinatorial background. It seems to be large enough for π^0 mesons. However for Λ hyperons the situation should be favorable (as it follows from already available experiments).

Fig.5 presents the dependence of the efficiency for all the particles from decay (2) to occur in the angular acceptance of the setup (in one projection). Three curves correspond to three

values of the Feynman variable x_F for Ξ_b^- . Quite similar results are obtained for process (3). The angular aperture of the setup is chosen to be $\nu = \pm 75$ mrad to provide the Ξ_b^- -baryon detection almost up to $x_F = 0$ with an efficiency $\epsilon = 80\%$.

Table VI. The decays of strange-beauty Ξ_b^- baryons

Decay type	Mean life (sec)	Decay probability
$\Xi_b^- \rightarrow \Xi_c^+(2460) \pi^- \pi^-$ (2) \downarrow $\Xi^- \pi^+ \pi^+$ \downarrow $\Lambda^0 \pi^-$ \downarrow $p \pi^-$	10^{-12}	2%
	$0.9 \cdot 10^{-12}$	7.5%
		100%
		64%
		10^{-3} (total probability)
$\Xi_b^- \rightarrow \Lambda_c^+ K^- \pi^-$ (3) \downarrow $K^- p \pi^+$	10^{-12}	0.5%
	$0.15 \cdot 10^{-12}$	7%
		$0.35 \cdot 10^{-3}$ (total probability)
$\Xi_b^- \rightarrow S(2560) \pi^- \pi^-$ (4) \downarrow $\Xi_c^+ + \gamma$ \downarrow $\Xi^- \pi^+ \pi^+$ \downarrow $\Lambda^0 \pi^-$ \downarrow $p \pi^-$	10^{-12}	2%
	$\sim 10^{-21}$	100%
	$0.9 \cdot 10^{-12}$	7.5%
		100%
		64%
		10^{-3} (total probability)

The setup was simulated at different values for the magnetic field integrals in magnets M1 and M2 and for its different configurations, which were determined by the distances between the magnets centers and dimensions of the main detector. Basing on the results of these calculations we have chosen the configuration of the facility presented in fig.3 and in Table V.

The decay length charmed and beauty particles make up from some fractions of a centimeter up to tens of centimeters (fig.6). With the target about 5 mm thick a considerable

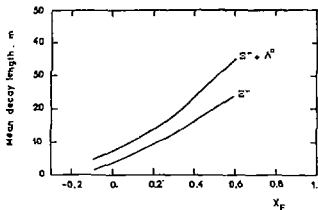


Fig. 4.
Average decay path of secondary hyperons, produced in decays (2) versus $X_F(\Sigma_B^-)$.

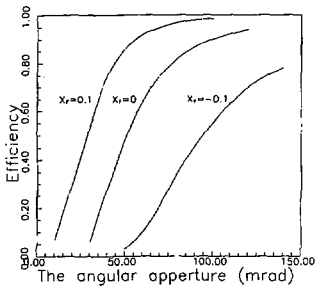


Fig. 5.
Efficiency of all the particles from decay (2) to occur in the angular acceptance of the setup for three values of $X_F(\Sigma_B^-)$.

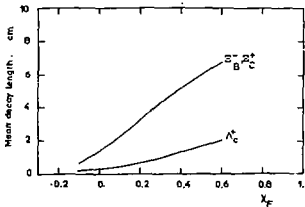


Fig. 6.
 Σ_B^- range and that of secondary charmed baryons Σ_C^+ and Λ_C^+ in decays (2), (3) versus $X_F(\Sigma_B^-)$.

fraction of the decays will occur outside the target. The length of the area for the vertex reconstruction with the aid of the vertex detector should be not less than 5-10 cm. The length for the strange hyperon decay reconstruction (Σ^- , Λ) should be not less than 15 m (and in a number of experiments not less than 30-50 m).

The multiplicity of the secondary charged particles in the events with the production and decay of particles with b quarks varies from 14 up to 35, the mean multiplicity is about 22 (fig.7). A very high resolution between the trajectories is required because of a high angular density of secondary particles (fig.8). When calculating the resolution of the spectrometer in momentum and effective mass we assumed that gas coordinate track detectors spatial resolution is 150 μm (DC1), 200 μm (DC2, DC3) and <300 μm (DC4) and energy resolution for the hadron calorimeters is $\Delta E/E = 100\%/\sqrt{E}$ [GeV]. The gaps between the detectors in the setup are to be filled with helium bags whose mylar walls are 100 μm thick. The total amount of the matter in the setup makes up to 15% from the nuclear interaction length and about 50% of radiation length.

The reconstruction of the simulated events includes:

1. the reconstruction of the charged particle trajectories by the given "hits" of the coordinate detectors;
2. the determination of the particle momentum and energy; having several measurements (2 magnets, calorimeter) we averaged the result with an account of the relevant errors;
3. step-by-step reconstruction of secondary vertices and the trajectories of the particles produced in these vertices.

In the effective mass calculations the particles emitted from the vertex were assigned the tabulated mass values.

To find the vertex one needed at least two trajectories to cross. The reconstruction of the momentum vectors of all secondaries was required for the determination of the effective mass. In the case one of the particles was missed, one had to reconstruct the momentum vector of this particle. This requirement is rather important for the reconstruction of the $\Sigma^- \rightarrow \Lambda \pi^-$ decays. If only Σ^- and π^- momenta are measured in the decay range, then by assigning the mass of Λ to the missed particle, one can reconstruct the effective mass of the

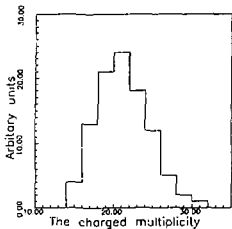


Fig. 7.
Multiplicity distribution for the secondary charged particles after the b and c particle decays. The multiplicity of particles accompanying bb pair was calculated with the LUND model (see the text).

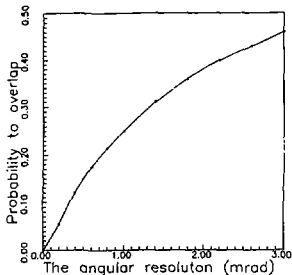


Fig. 8.
The probability of sticking of the selected track to some other track of the given event versus the detector angular resolution.

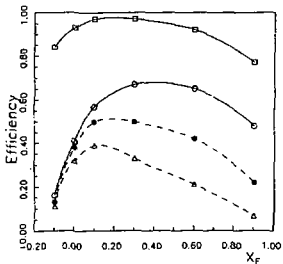


Fig. 9.
The Σ_B detection efficiency in decays (2) and (3) versus X_F .
O - decay (2), where the Σ and Λ may not be defined; ● - events of decay (2) with measuring Σ masses; Δ - events of decay (2) with measuring Σ and Λ masses; □ - events of decay (3).

candidate for Ξ^- . The background events of a similar configuration $\Xi^-n\pi^-$ correspond to the effective mass of the "candidate for Ξ^- ", which is by 50 MeV higher than the true one. Hence for the reliable reconstruction of Ξ^- the setup should have the Ξ^- mass resolution in the events with a missed Λ not worse than 10-15 MeV, which indeed can be realized.

The particle which managed to decay, were considered to be detected, if one could reconstruct their effective masses within certain limits w.r.t. their true mass values:

$$\Delta m(\Xi_b^-) = \pm 50 \text{ MeV}, \Delta m(\Xi_b^0) = \pm 50 \text{ MeV}; \Delta m(\Xi^-) = \pm 20 \text{ MeV}; \Delta m(\Lambda^0) = \pm 20 \text{ MeV}.$$

Three classes of the events were treated:

- a) both effective masses of Ξ^- and Λ could be not reconstructed;
- b) Ξ^- hyperon effective mass was reconstructed, but that of Λ hyperon could be not;
- c) both effective masses must be determined.

The detection efficiency of Ξ_b^- for two decay channels (2) and (3) are presented in fig.9. The efficiencies for the events of classes a)-c) are presented separately for decay (2). Consequently the efficiency is more than 40% for decay (2) and more than 80% for decay (3) at $x_p > 0$.

The efficiency of reconstruction of radiative decay (4) with soft photon ($\langle E_\gamma \rangle \approx 5 \text{ GeV}$ at $x_p(\Xi_b^-) \approx 0$) is $\approx 30\%$.

The effective mass resolution for Ξ_b^- (fig.10) is within the limits 12-30 MeV for decay (2) and 10-20 MeV for decay (3). Coulomb scattering is important in mass resolution calculations.

4. RESEARCH PROGRAM

4.1. Study of Heavy Quark Physics

Up to now the principal investigations of the properties of the particles with heavy quarks, and first of all, the studies of B meson weak decays, were mainly carried out at the e^+e^- storage rings. These experiments provide favorable background conditions, caused by an considerable contribution to heavy flavor production mechanism made by some vector mesonic states

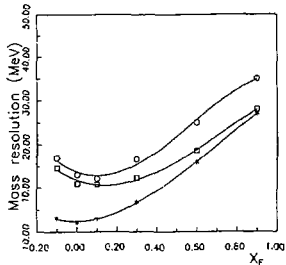


Fig. 10. Effective mass resolution when detecting decays (2) and (3). \circ - decay (2), \square - decay (3), $*$ - decay (3) with no account of multiple scattering.

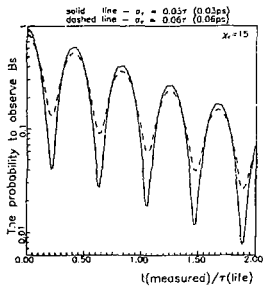


Fig. 11. Observation of space oscillations $B^0 - \bar{B}^0$ at different accuracies of measuring the proper decay time for B^0 -mesons

with hidden charm or beauty, which are well produced in e^+e^- -collisions ($e^+e^- \rightarrow \phi(3770) \rightarrow D\bar{D}$ and $e^+e^- \rightarrow T(4S) \rightarrow B\bar{B}$). Interesting possibilities arise also here in the Z boson resonance production on the LEP and SLC machines. At present e^+e^- beam experiments the sensitivity corresponds to the production of several hundreds of thousands of B mesons, D mesons and τ leptons. The projects for the b and c - τ factories are in progress now, which will allow one to increase the luminosity at least by an order of magnitude.

Table VII. Comparison of B-meson yields at different accelerators.

Accelerator; experiment	\sqrt{s} , GeV	Luminosity	$\sigma(b\bar{b})$, nb	$\frac{\sigma(b\bar{b})}{\sigma(\text{tot})}$	$N(b\bar{b})$	N_τ
^{a)} $e^+e^- \rightarrow Y(4S) \rightarrow B\bar{B}$ (5)	10.6	$10^{33} \text{ cm}^{-2} \text{ s}^{-1}$	1	0.25	10^7	$4 \cdot 10^{7**}$
LEP: $e^+e^- \rightarrow Z^0 \rightarrow B\bar{B}$	92	$10^{31} \text{ cm}^{-2} \text{ s}^{-1}$	5	0.15	$6 \cdot 10^5$	$3 \cdot 10^5$
^{b)} BCD, Tevatron (6)	1800	$10^{31} \text{ cm}^{-2} \text{ s}^{-1}$	$45 \cdot 10^3$	10^{-3}	$4 \cdot 10^9$	
E-777 Tevatron, fix. target (7)	40	10^6 s^{-1} interactions	20	$5 \cdot 10^{-7}$	$4 \cdot 10^6$	
^{c)} SSC proton beam experiment (8)	200	10^7 s^{-1} interactions	$2.5 \cdot 10^3$	$2 \cdot 10^{-4}$	$2 \cdot 10^9$	
^{d)} UNK hyperon ex- periment	72	10^6 s^{-1} interactions	300	$7 \cdot 10^{-6}$	$4 \cdot 10^7$	$5 \cdot 10^7$

Notes: 1. The expected rate of the $N(b\bar{b})$ events per 100 days of the accelerator operation is given.

2. In the fixed target experiments it was assumed that for the nuclei $\sigma(\text{nb})/\sigma_{\text{tot}} \sim A^{0.3}$ (for Si). It has been

taken into account in the estimates of $N(b\bar{b})$.

3. The UNK duty factor is 30 %.

4. (*) implies that this is project.

5. The experiment on the SSC proton beam foresees the extraction of the proton beam with an intensity up to 10^9 p/s using a bent crystal.

6. (**) " c - τ " factories.

On the other hand, the experiments on the studying heavy particles in hadronic beams (fixed target experiments) are becoming more and more important. The projects of B-decay studies using hadron colliders are also being prepared. Table VI presents the expected yields for charmed and beauty particles for different types of the machines.

This Table allows one to make the following conclusions:

1. At present one cannot unambiguously point out the most promising ways for the development of B meson physics (see the discussion in [9]). However it seems that the experiments at the SNS proton beam and at the hadron colliders are the most suitable ones for the search of CP violation effects in the B decays, which require luminosity corresponding to $>10^9$ $B\bar{B}$ pair production. Under the UNK conditions the experiments in the intense proton beam ($>10^{11}$ ppc) with specialized facilities, which are capable to select definite rare decay channels of B mesons in a comparably narrow range of the phase space, may be quite competitive.

Large CP-violation effects may be expected in such decays. For instance, we are now clarifying possibilities of measuring the asymmetry in $\Gamma(B^+ \rightarrow p\bar{p}\pi^-)$ and $\Gamma(B^+ \rightarrow p\bar{p}\pi^+)$, $\Gamma(B^- \rightarrow K^-\phi)$ and $\Gamma(B^- \rightarrow K^-\bar{K})$

$\Gamma(B^+ \rightarrow K^+\phi)$, $\Gamma(B^0 \rightarrow K^-\pi^+)$ and $\Gamma(B^0 \rightarrow K^+\pi^-)$ and for some other rare decay channels when normalizing them over main decays of

the type $B^- \rightarrow D^0\pi^-$ and $B^+ \rightarrow D^0\pi^+$, for which the asymmetry should be very small (i.e., the search for the differences in the ratios

$$\left[\frac{\Gamma(B^- \rightarrow p\bar{p}\pi^-)}{\Gamma(B^- \rightarrow D^0\pi^- \rightarrow K^-\pi^+\pi^-)} - \frac{\Gamma(B^+ \rightarrow p\bar{p}\pi^+)}{\Gamma(B^+ \rightarrow D^0\pi^+ \rightarrow K^+\pi^+\pi^-)} \right] \text{ etc.}$$

Such experiments may be carried out in the underground hall for the hyperon beam where one can perform investigations with high intensity protons using specialized facilities with precise measurement of the effective masses of the final states (e.g., as it was done in ref. [10], where the accuracy of $\Delta m/m =$

= 0.0017 was obtained, and this accuracy can be increased several times).

2. The experiments with D and B mesons and searches for CP-invariance violation may be carried out at the accelerators of different types, however hadron beams have very great advantages in the search and study of charmed and beauty baryons and their weak decays. There are no highly effective mechanisms of heavy baryon production for the colliding e^+e^- beams. In the experiments at the pp colliders one can hardly realize the conditions necessary for the selection of complicated cascade processes, required for the search of baryon states with heavy quarks and for a thoroughly study of the characteristics of their weak decays. Hadronic accelerators of the UNK type may be extremely useful for such experiments. In particular, the UNK hyperon beam opens new possibilities for the experiments with strange-beauty and strange-charmed baryons (Qsq and Qss ; $Q=c$; b) which up to now have not practically been investigated.

The results of two experiments where Ξ_c^+ baryon was observed may be a good evidence in favor of the advantages of the hyperon beams as far as the study of baryonic (Qsq) states is concerned.

a) WA-62 experiment (CERN Σ^- beam, $P_\Sigma = 135$ GeV/c (11))

$$\sigma(\Sigma^- + Be \rightarrow \Xi_c^+ + X) |_{x_p > 0.6} \cdot BR(\Xi_c^+ \rightarrow \Lambda K^- \pi^+ \pi^+) = (5.3 \pm 2.0) \mu\text{b}/\text{Be},$$

$$(dN/dx_p dp_T^2) = \text{const} \cdot \exp(-bp_T^2) (1-x)^n; \quad b = 1.1_{-0.4}^{+0.7} (\text{GeV}/c)^{-2};$$

$$n = 1.7 \pm 0.7.$$

b) E400 experiment (FNAL neutron beam, $\langle E_n \rangle = 600$ GeV (12))

$$\sigma(n + N \rightarrow \Xi_c^+ + X) |_{0 < x_p < 0.6} \cdot BR(\Xi_c^+ \rightarrow \Lambda K^- \pi^+ \pi^+ + \Sigma^0 K^- \pi^+ \pi^+) =$$

$$= \left[7.5_{-3.6}^{+4.5+1.9} - 1.9 \right] \mu\text{b}/\text{nucleon},$$

$$(dN/dx_p dp_T^2) \approx \text{const} (1 - x_p)^n \exp(-bp_T^2); \quad b = 0.97 \pm 0.21 (\text{GeV}/c)^{-2};$$

$$n = 4.7 \pm 2.3 \text{ (for } 0.15 < x_p < 0.6); \quad \sigma \propto A^{0.90 \pm 0.13}.$$

The comparison of these experiments whose results differ at least several times (or even ten times) when extrapolated over

the whole range of x_F , show that in the hyperon experiments production processes of strange-charmed baryons may be characterized by considerably larger cross sections or by a more smooth x_F distribution contrary to the NN collisions. These ideas have theoretically been grounded in ref. [13].

For $x_F > 0.5 - 0.6$ there are more pure conditions for the search of new baryon states as compared with central production processes. All these make us think that the hyperon experiments open unique possibilities in the search and study of baryon states with heavy and strange quarks. These possibilities are beyond any competition with experiments at other types of accelerators and beams.

Though it would be much more easier to construct a spectrometer working in the region of large x_F (just because of smaller sizes of the detectors), however we plan to have a set-up, which would allow us to carry out investigations in a wide range of $0 < x_F < 1$, and consequently we will be able to considerably enrich our experimental program.

Let us enumerate now the main directions in the heavy particle physics to be realized with the UNK hyperon beam.

4.1.1. Spectroscopy of Strange-Beauty and Strange-Charmed Baryons.

a) Search and study for baryons of the (Qsq) type with strange and heavy quarks and their excited states

$$\Xi_c^+ \equiv (usc)^+; \Xi_c^0 \equiv (dsc)^0; \Omega_c^0 \equiv (ssc)^0; \Omega_{cc}^+ \equiv (scc)^+.$$

$$\Xi_b^0 \equiv (usb)^0; \Xi_b^- \equiv (dsb)^-; \Omega_b^- \equiv (sbb)^-; \Omega_{cb}^0 \equiv (srb)^0.$$

b) Study of complicated cascade decays of these baryons, acquiring detailed information about concrete exclusive decay channels and their characteristics (decay probability, asymmetry parameters, etc.). It is required to reconstruct a number of cascade decay vertices in these experiments.

c) Precise measurements of the lifetime of charmed and beauty hadrons.

d) Determination of the matrix elements for K.M. matrix. Note, that because of the difficulties in theoretical description of the decay processes (deviations from the spectator model) one

needs for the definition a wide set of experimental data on baryon and meson decays.

Table VIII presents the data, which allow one to estimate the capability of the proposed experimental program to observe a number of new strange-charmed and strange-beauty baryons and to study their weak leptonic and nonleptonic decays. As it follows from the Table one can obtain an extremely detailed information about many processes. For instance, one can study weak cascade decays (2) and (3). Table VI by detecting $(1+2) \cdot 10^3$ completely identified events of (2) and (350-700) events of (3). It will also be possible to detect a number of other nonleptonic decay channels and to obtain data on leptonic decays



(BR $\sim 1.5 \cdot 10^{-3}$, N $\sim 3 \cdot 10^3$ events)

or



(BR $\sim 3 \cdot 10^{-3}$, N $\sim 5 \cdot 10^2$ events).

We can easily go on with this list using Table VIII and estimates for branching of separate channels from ref. (4).

It is of interest to look for excited states of charmed-strange, and, maybe, beauty-strange baryons which may decay with further emission of π mesons or photons. To improve the background conditions one should carry out these experiments in the region of $X_p > 0.5$.

A possibility to observe radiative decays of strange-charmed excited baryons produced in the cascade decays of heavier beauty baryons (see(4)) was also considered. Because of kinematic

constraint more pure background conditions for the search of radiative decays may be realized. The calculations, which take into account the detection of photons from radiative decays $S_c(2560) \rightarrow S_c(2460) + \gamma$ in the electromagnetic calorimeters of the facility, made it clear that 500-1000 events of decay (4) might be detected in the experiment if allowed by the background conditions.

It goes without saying that alongside with all these data we shall obtain rich statistics for the study of heavy hadrons not containing strange quarks.

Table VIII. Statistics for the events with charmed and beauty particles.

Process	Cross section $\sigma(X_p > 0)$ (cm^2)	$(ZBR)_{\text{th}}$	$N_{\text{nonlep. per 100 days of measurements}}$	$(ZBR)_{\text{exp}}$	$N_{\text{lep. per 100 days of measurement}}$
$\Sigma^- + N \rightarrow \text{cc} + X$	$(1 \pm 2) \cdot 10^{-28}$		$\sim 5 \cdot 10^9$		
$\Sigma^- + N \rightarrow (\text{scu})^+ + X$ $(\text{scd})^0 + X$	$(1 \pm 2) \cdot 10^{-29}$	0.05 ± 0.10	$3 \cdot 10^7 \pm 10^8$	0.10	10^8
$\Sigma^- + N \rightarrow (\text{ssc})^0 + X$	$(1 \pm 2) \cdot 10^{-30}$	0.15 ± 0.20	$10^7 \pm 2 \cdot 10^7$	0.04	$5 \cdot 10^6 \pm 10^7$
$\Sigma^- + N \rightarrow (\text{scs})^+ + X$	$\sim 10^{-34} \cdot 10^{-33}$	~ 0.02	$\sim 10^2 \pm 10^3$	~ 0.02	$\sim 10^2 \pm 10^3$
$\Sigma^- + N \rightarrow \text{bb} + X$	$(3 \pm 5) \cdot 10^{-31}$		$2 \cdot 10^7 \pm 4 \cdot 10^7$		
$\Sigma^- + N \rightarrow (\text{bcu})^0 + X$ $(\text{bcd})^+ + X$	$\sim 3 \cdot 10^{-32}$	~ 0.005	$\sim 10^4$	~ 0.015	$\sim 3 \cdot 10^4$
$\Sigma^- + N \rightarrow (\text{bcc})^+ + X$	$\sim 3 \cdot 10^{-33}$	~ 0.01	$\sim 2 \cdot 10^3$	~ 0.02	$\sim 4 \cdot 10^3$
$\Sigma^- + N \rightarrow (\text{bcs})^0 + X$	$\sim 3 \cdot 10^{-38}$	~ 0.01	$\sim 10^{-2}$		
$\Sigma^- + N \rightarrow D_s^0 + X$	$\sim 6 \cdot 10^{-32}$	~ 0.01	$\sim 4 \cdot 10^4$	~ 0.015	$\sim 6 \cdot 10^4$
$\Sigma^- + N \rightarrow D_s^+ + X$ $\downarrow \rightarrow \tau^+ \nu_\tau$	$(2.5 \pm 5) \cdot 10^{-29}$			0.02 ± 0.04	$5 \cdot 10^7 \pm 2 \cdot 10^8$

- Notes: 1. The data on the production cross sections for heavy particles are rather ambiguous, and the relevant theoretical estimates admit considerable arbitrariness. The values for $\Sigma^+N \rightarrow c\bar{c}+X$ we used, are several times lower than those which can be obtained from the data extrapolation [11] and are about an order of magnitude larger than the theoretical estimates of ref.[14]. The ratio $\sigma(\Sigma^+N \rightarrow b\bar{b} + X)/\sigma(\Sigma^+N \rightarrow c\bar{c} + X) \approx 3 \cdot 10^{-3}$ and the ratios between production cross sections for different types of heavy hadrons [14] were used alongside with the ratio $\sigma(\Sigma^+N \rightarrow (scc) + X)/\sigma(\Sigma^+N \rightarrow (scu)+X) \approx 10^{-4}-10^{-5}$. The last ratio was obtained in the model of independent production of two c -quarks (in ref.[15]) this ratio is estimated as 10^{-5} . It should be noted, that ref.[13] gives a considerably larger cross section for (bcu) baryon productions, as compared with that in the Table.
2. It is assumed that $I(\Sigma^-) \approx (1-2) \cdot 10^7 \Sigma^-/s$, and the Si target is $(1/10) + (1/20)$ of the interaction length, i.e., we have $10^6 \Sigma^-N$ interactions/s. The application of the $\sigma(b\bar{b}, c\bar{c}) \propto A^1$ dependence increases the statistics for the Si target three times (this value was taken into account in calculating the number of events).
3. The average efficiency of detecting heavy particle decays is ≈ 0.25 (which has also been taken into account in the calculations).
4. $(ZBR)_h$ is the total probability for all nonleptonic decays of a relevant heavy state into charged particles and Λ^0 hyperons only. $(ZBR)_{\mu+e}$ is the total probability for leptonic decays of heavy particles $R = [X(n^+)e^- \bar{\nu}_e + X(n^+)\mu^- \bar{\nu}_\mu]$ with completely identified hadronic states decaying into charged particles only. $(ZBR)_h$ and $(ZBR)_{\mu+e}$ have been determined from theoretical estimates [4].
5. $(scu) \equiv \Sigma_c^+$, etc., are strange-charmed and strange-beauty baryons; $B_s^+ = (s\bar{b})$.

4.1.2. Study of the Mixing Effects in the System of Neutral B Mesons*

Let us consider in more detail the search for spatial $B_S^0 \leftrightarrow \bar{B}_S^0$ oscillations. B_S^0 mesons are produced in the reaction

$$\Sigma^- + N \rightarrow B_S^0 + \begin{cases} (b\text{-baryon}) + X \\ B^0 + X \\ B^- + X \end{cases} \quad (7)$$

The time dependence of the number of B_S meson decays has the form

$$N_{B_S^0}(t) = \left[N_{B_S^0}(0)/2 \right] \exp(-t/\tau) [1 + \cos(\chi_S \cdot t/\tau)]. \quad (8)$$

Here τ is the life-time of B_S (in the rest frame), $\chi_S = \Delta m \cdot \tau$ - oscillation parameter. In the framework of the Standard Model using the data on B_d^0 - \bar{B}_d^0 -mixing one obtain the prediction

$$\chi_S \approx |V_{ts}/V_{td}|^2 \cdot \chi_d \approx 15. \quad (9)$$

Whereof it follows that the value for the parameter of integral mixing of B_S^0 -mesons r_S is expected to be close to unit

$$r_S = \chi_S^2 / (\chi_S^2 + 2) \approx 0.99. \quad (10)$$

Therefore one will not be able to determine χ_S with a reasonable accuracy when measuring integral mixing. Direct experiments on observing spatial oscillations are required for χ_S measurements. For this purpose one should measure the time-of-flight distributions for B_S^0 and momenta of these particles (to identify B_S^0 and to determine time in B_S^0 rest frame) and tag initial $B_S^0 = (b\bar{s})$ by their flavor. The tagging can be realized by the charge sign of the associative b-particle or by the charge sign of a lepton in the associative particle decay. To measure the B_S^0 meson momentum one should single out its fully reconstructable modes (see Table VIII). As it follows from the tagging efficiency estimates, it is $\epsilon(\text{tag}) \approx \epsilon(\text{associative particle}) \approx 0.20 \cdot 0.5 \approx 0.1$. Therefore the total sta-

*For discussion of mixing and CP violation in B-meson decays see e.g., [9,16-20].

tistics for such tagged one reconstructed B_s^0 decays will make up $5 \cdot 10^3$ per 100 days of the accelerator operation, which is quite sufficient for spatial oscillations measurements. The accuracy in measuring the life-time in B_s^0 rest frame is mainly determined by the accuracy in measuring the decay path in the vertex detector. It is expected that $\delta t(B_s^0) = 0.5 \cdot 10^{-13}$. The limited resolution leads to the smearing of the observed oscillations (see fig.11). The planned experiment allows for the measurement of x_s in the range of its $3 < x_s < 30$. At $x_s \sim 15$ (the theoretically expected value) the accuracy of its measurement $\delta(x_s)$ will be several percent.

4.1.3. Search for Rare and Forbidden Heavy Particle Decays.

The experiments with B and D mesons as well those with τ leptons open new possibilities in the search for rare processes caused by lepton charge nonconservation, contribution from weak neutral currents with flavor nonconservation (PCNC) or by some other new processes ($B_{S; d}^0 \rightarrow \mu^+ \tau^-$, μe ; $B \rightarrow \mu^+ X^-$; $\tau \rightarrow \mu$; $\tau \rightarrow \mu e^+ e^-$; $B_{S; d}^0 \rightarrow \mu^+ X^-$; $D^0 \rightarrow \bar{D}^0$ et al.; the τ leptons are produced in the $D^{\pm} \rightarrow \tau^{\pm} \nu_{\tau}$ decays, see Table VIII). Here the search for lepton charge nonconservation in the transition between the third and second, third and first or to all the three generations of fundamental particles are of primary interest. Up to now a sensitive check of lepton charge conservation was realized only for the transitions between members the second and first fundamental generations ($\mu \rightarrow e \gamma$; $3e$) or within one generation (double β decay). It should be noted here that in the models with the Higgs mechanism of lepton charge nonconservation the extent of this nonconservation sharply increases with the growth of lepton mass. Therefore, e.g., $BR(B \rightarrow s \tau \mu) < 10^{-7}$ will be equivalent in its sensitivity to $BR(K_L^0 \rightarrow \mu e) < 10^{-14}$ (the present limitation is $BR(K_L^0 \rightarrow \mu e) < 3 \cdot 10^{-10}$, and it hardly possible that this branching will be brought below $10^{-11} - 10^{-12}$ in the near future).

Hence the study of weak decays of heavy particles in the UNK hyperon beam may play an important role in the investigations of a number of fundamental problems of elementary particle physics, which are:

A. A precise check of the Standard Model (unitarity of the quark mixing matrix).

B. Search for the effects going beyond the SM framework: new currents, low energy manifestations of new superheavy fundamental particle families, "horizontal" gauge and Higgs bosons.

C. Study of CP-violation.

D. Study of QCD predictions in the decay of heavy particles both at small distances and in the range of large distances, corresponding to soft processes and confinement effects. Weak decays of heavy particles (especially with the b-quark) are one of the most pure laboratories for the study of strong interactions, since the initial states determined by the weak processes are given.

Note, that a different approach to the manifestation of the confinement and QCD problems may be found in the study of exotic hadronic states and, in particular, of strange-charmed and strange-beauty exotics. These manifestations are considered below

4.2. Search for Heavy Exotic Hadrons

During last years there was quite a noticeable progress in the experiments on search for exotic hadrons: multiquark mesons ($qq\bar{q}\bar{q}$) and baryons ($qqqq\bar{q}$), glueballs (gg) and mixed states of a hybrid type ($q\bar{q}g;qqqg$). The study of the systems of strongly interacting particles consisting of light u,d,s quarks resulted in the observation of several states, whose properties could not be described in the framework of a ordinary quark model for hadrons (i.e., $q\bar{q}$ mesons and qqq baryons). These states are considered now to be strong candidates for exotic particles (see, e.g. [21,22]). Most of these candidates are cryptoexotic hadrons.

At the UNK energies the search for exotic hadrons may greatly be extended, since then they will include multihadronic states with heavy c and(or) b quarks. A larger number of the types of quarks may bring us to new interesting possibilities. In ref.[23] a principle of flavor antisymmetry was formulated, according to it the most strongly connected states are those consisting of two quarks (or of two antiquarks) with different flavors. Then for the mesons of the type $qq\bar{q}\bar{q}$:

a) the lightest scalar states consisting of $q=u,d,s$ have usual values of the quantum numbers; it is possible that ρ and S^* mesons are such cryptoexotic states;

b) the lightest scalar strange-charmed mesons may have open exotic sets of quantum numbers (since now quarks are characterized by 4 different flavors).

In refs. [24,25] it has been shown that there may exist exotic baryons with strange quarks and charmed antiquarks of ($\bar{c}qqqs$) or ($\bar{c}qqss$) types, which with a large probability may be stable w.r.t. strong and electromagnetic interactions. Such a situation may also take place for ($bqqqs$) baryons. The examples of the exotic states with heavy quarks are given in Addendum I (see Table XVII; see also [26]). In what follows let us consider some new opportunities, connected with the search for the exotic and cryptoexotic states with open and hidden beauty and charm.

The search for cryptoexotic states occupy a particular place in the studies of nanobarn hadronic spectroscopy. Since one can judge about complicated inner structure of cryptoexotic mesons and baryons only by indirect dynamic features (anomalously-small widths, anomalous decay branchings, special production mechanisms) the corresponding experiments will be quite difficult. Here we are speaking about the processes with small cross sections, whose identification is possibly only in the case they are characterized with bright signatures, which allow to reliably single out a signal against background. The success in the study of exotic hadrons with light quarks was caused, to a great extent by proper choice of exclusive processes for their production and specific decay channels.

At the energies of 1-3 TeV the cross sections of the most exclusive two-particle reactions, used in the experiments with light mesons at moderate energies (below 100 GeV), become very small. Therefore such processes can no longer be effective for the search of exotic hadrons in a new energy range. However we should mention here some mechanisms which may successfully be used in the search for heavy exotic hadrons at high energies both in hyperon beams and in proton and π meson beams. These beams will also be extracted into the area of the setup location. Such a wide set of the beams will allow one to carry out a systematic search for exotic heavy hadrons at the UNK accelerator. The corresponding production mechanisms for exotic hadrons are presented in Table IX.

The experiments on the study of exotic heavy hadrons when they are produced following quasi-exclusive and diffraction mechanisms (1° and 2°) are very much similar and correspond to the operation in the spectrometer mode for forward going particles. The facility will be arranged in the same way for the investigation of the Coulomb production processes 3° . The general scheme of the setup does not change greatly, however it stretches along the beam up to 150 m. Table X presents the estimates of the experimental possibilities for the relevant processes. Particle production in the Coulomb field of a nucleus is discussed in detail in Appendix 2. Note that contrary to $2^\circ - 4^\circ$ mechanisms 1° and 5° may result in the production of multiquark hadrons with open exotics.

Table IX. Exotic Hadron Production Mechanism at Very High Energies

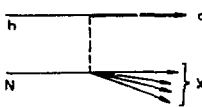
<p>1°. Quasi-exclusive Processes</p> $h+N \rightarrow a + X_{\text{lower vert.}} \quad (11)$ <p style="text-align: center;"> $X_p > 0.8 + 0.9$ </p> 	<p>From qualitative considerations one may assume that the cross sections for these processes do not decrease rather rapidly with energy. In this at very high energies the particles from upper and lower vertices are well separated over their rapidities, i.e., the inclusive character of the reaction in the lower vertex does not produce undesirable background in the identification of decays for 'a' particles. No experimental data are available at present on the energy dependence of such quasiexclusive cross sections. However it has been shown that they are much larger than the cross sections for corresponding two-body reaction. (see discussions of these problems in refs. [21,27]).</p>
---	---

Table IX (continued)

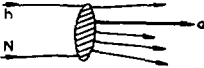

<p>Exotic hadron production in fragmentation region (large x_F)</p> $h+N \rightarrow \begin{matrix} a \\ \bar{P} \end{matrix} > 0.5 + 0.6^{+X} \quad (12)$ 	<p>The inclusive mechanism of exotic hadron production in the fragmentation region of an incident particle is very close to the quasiexclusive process discussed above. As compared with all other inclusive reactions in this fragmentation region at sufficiently large x_F, one may expect more favourable conditions for the selection of resonances because of the reduction of the combinatorial background. It is more true if the charge of the produced hadronic state a differs from that of an incident particle. This situation holds in the experiments where indications to a possible existence of U mesons were obtained [28,29]. Hyperon beams allow one to search here for the particles with strange quarks, e.g., strange-charmed exotic: \bar{P} and \bar{P}_s mesons or P_{cs} baryons (see Table XVII in Appendix I).</p>
<p>2°. Diffractive hadron production (pomeron exchange)</p> $h+N \rightarrow a+N. \quad (13)$ <p>Here the flavors of h and a must be the same.</p> 	<p>A possibility for such production mechanism of exotic states with the cross sections of about $\sim 1 \mu\text{b}$ was treated in [30] in connection with the model of the existence of cryptoexotic component of the pomeron. According to the modern notions, pomeron is a multigluon system, which confirms the possibility of exotic hadron production in diffractive processes. It is also of interest to study cascade processes, e.g., diffractive production of a baryon system and its decay with exotic meson production. Systematic search for exotic hadron production in diffractive processes are still in progress. However it is quite possible that a baryon with hidden strangeness N_s (1960) observed in the BIS JINR experiments is produced namely due to such a diffractive mechanism [31].</p>

Table IX (continued)

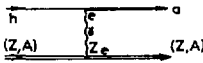
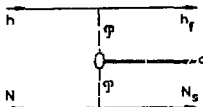
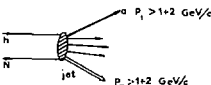
<p>3°. Particle production in the nucleus Coulomb field</p>  <p>$h(Z, A) \rightarrow a(Z, A)$ (14)</p>	<p>Coulomb production processes are of great interest both for the search of exotic hadronic states [32], and for the study of Coulomb excitation of the known hyperon resonances.</p>
<p>4°. Central production of exotic states (double pomeron exchange)</p> <p>$h+N \rightarrow h_f + N_s$ (a-hadrons) N_s (15)</p> 	<p>This mechanism was treated in detail in the experiments of the GAMS group and the GLUON project [33] is based on it. In connection with the problems on the existence of exotic mesons with charmed and beauty quarks, this mechanism may be of great interest for the search for hybrid mesons (ccg) of (bbg). The hyperon beam seems to have no advantages as compared with π or p beams (only if the spectrum of sea gluons in hyperons be not more hard).</p>
<p>5°. Exotic hadron production in large p_T processes</p> <p>$h+N \rightarrow a(p_T > 1+2 \text{ GeV}/c) + \text{jet}(p_T > 1+2 \text{ GeV}/c) + X$ (16)</p> 	<p>In the large p_T processes the production of exotic states with excited complicated color inner structure may be singled out more clearly than in other reactions.</p>

Table X. Search and Study of the Production of Exotic Hadronic States

Process	BR	ϵ	Experimental results	Notes
1	2	3	4	5
1^0 $\Sigma^- + N^- \rightarrow (dd\bar{s}0\bar{0}) + H$ $\downarrow \text{L}\bar{\Sigma}^-$ $\downarrow l^+ l^- = \mu^+ \mu^-; e^+ e^-$	0.14	0.35	Experimental sensitivity is 600 events/nb (for $\sigma_{\text{dir}} \text{BR}((dd\bar{s}0\bar{0}) \rightarrow \mu\bar{\mu})$).	Diffractional production of exotic baryons with heavy quarks (with hidden exotics)
2^0 $\Sigma^- + N^- \rightarrow (dd\bar{s}b\bar{b}) + H$ $\downarrow \text{L}\bar{\Sigma}^-$ $\downarrow l^+ l^- = \mu^+ \mu^-; e^+ e^-$	0.05	0.35	Experimental sensitivity is 200 events/nb (for $\sigma_{\text{dir}} \text{BR}((dd\bar{s}b\bar{b}) \rightarrow \mu\bar{\mu})$).	
3^0 $\Sigma^- + N^- \rightarrow \left[\begin{array}{l} \text{M}_{\phi}^{(1)} \\ \downarrow \phi\pi; \phi\pi \end{array} \right] + X$ $\downarrow \text{L}\bar{\Sigma}^-$ $\downarrow l^+ l^- = \mu^+ \mu^-; e^+ e^-$ $x_p > 0.5$	0.14		Experimental sensitivity: 600 events/nb (for $\sigma _{x_p > 0.5} \cdot \text{BR}[\text{M}_{\phi}^{(1)} \rightarrow \phi\pi; \phi\pi]$).	Quasi-exclusive production of mesons and baryons with heavy quarks and their production in the fragmentation region ($x_p > 0.5 + 0.8$).
$\left[\begin{array}{l} \text{M}_{\phi\bar{K}} \\ \downarrow \phi\bar{K}^+ K^- \end{array} \right] + X$ $\downarrow \text{L}\bar{\Sigma}^-$ $\downarrow l^+ l^- = \mu^+ \mu^-; e^+ e^-$ $x_p > 0.5$	0.07 + 0.14		300-600 events/nb (for $\sigma _{x_p > 0.5} \cdot \text{BR}[\text{M}_{\phi\bar{K}} \rightarrow \phi\bar{K}^+ K^-]$).	
$\left[\begin{array}{l} \text{M}_{\bar{K}^0} \\ \downarrow \bar{K}^0 K^+ K^- \end{array} \right] + X$ $\downarrow \text{L}\bar{\Sigma}^-$ $\downarrow l^+ l^- = \mu^+ \mu^-; e^+ e^-$ $x_p > 0.5$	0.05		200 events/nb (for $\sigma _{x_p > 0.5} \cdot \text{BR}[\text{M}_{\bar{K}^0} \rightarrow \bar{K}^0 K^+ K^-]$).	

Table X (continued)

1	2	3	4	5
4^0 $\Sigma^- + N \rightarrow (\bar{u}uds) _{x_p > 0.5} + X$ $\downarrow p\bar{p}\pi^- ; \bar{p}\pi^+ ; \Lambda K^+ \pi^-$ $-(\bar{u}uds) _{x_p > 0.5} + X$ $\Sigma^- + N \rightarrow (s\bar{u}d) _{x_p > 0.5} + X$ $\downarrow \pi^+ \pi^+ K^- K^-$			$10^3 - 10^4$ events of this type for each process may be detected	<p>The exotic states are assumed to decay along weak channels - see Table XVII (VD experiment). It is also assumed that the production cross section for exotic anticharmed strange baryon is $\sim 10^{-2}$ from the cross section of Σ_c^+ or Σ_c^0 production. Besides $\sigma^1_{x_p} > 0.5 \sim 0.1 \sigma^1_{x_p} > 0$ (for $d\sigma/dx_p \sim \sim (1-x_p)^2$). In principle, the requirement $x_p > 0.5$ is not obligatory similarly as in the VD experiments on Σ_c^+; however it makes the conditions for the search of exotic hadrons more pure.</p>

Table X (continued)

1	2	3	4	5
5° $\pi^- + \text{Pb} \rightarrow \rho(1480)^- + \text{Pb}$ $\begin{array}{l} \downarrow \rho\pi \\ \downarrow K^+K^- \end{array}$ Similar processes for other exotic mesons, strongly connected with π channel, e.g. $\pi^- + \text{Pb} \rightarrow \rho(\rho^{3P_1} = 1^-) + \text{Pb}$ $\downarrow \rho\pi; \eta K^-; D(1285)\pi^-$ (see [32])	0.5	0.5	This process may be detected, if $\text{BR}[\rho(1480)^- \rightarrow \pi K^-] > 0.4 \cdot 10^{-2}$	Experiments on exotic meson production in the Nuclear Coulomb field. For details see Appendix I.
6° $\Sigma^- + \text{Pb} \rightarrow \Sigma(3170)_\phi^- + \text{Pb}$ $\begin{array}{l} \downarrow \Sigma^- K K + \pi \\ \downarrow \phi \Sigma^- \end{array}$	0.5	0.5	These studies allow one to solve the problem on the existence of a narrow $\Sigma(3170)_\phi^-$ baryon, if $\text{BR}[\Sigma(3170)_\phi^- \rightarrow \Sigma^- \pi] > 0.04 - 0.07$	
7° $\Sigma^- + \text{Pb} \rightarrow (\omega \bar{\omega} \bar{d} \bar{d} \bar{n})^- + \text{Pb}$ $\begin{array}{l} \downarrow \omega \Sigma^- \\ \downarrow \mu^+ \mu^-; e^+ e^- \end{array}$	0.14	0.5	The same if $\text{BR}[\Sigma(5000)_\omega^- \rightarrow \Sigma^- \psi] > 0.07$	

- Notes: a) The measurements are assumed to be carried out during 10 days ($3 \cdot 10^5$ s with an account of the accelerator duty factor) at the intensity of 10^7 particles/s.
- b) In processes 1-3 the measurements are made with a standard Be target 0.2 nuclear length.
- c) In processes 4 the measurements are made with an active target - $V\mathcal{D}$, similarly as in Σ_0^{++} , etc. study.
- d) Coherent processes in the Pb nuclear Coulomb field (5-7) are studied with the target 1.4 g/cm^2 ($4 \cdot 10^{21}$ Pb nuclei/cm 2).

4.3. Study of the Coulomb Production of Excited Hyperon States (Hyperon Radiation Widths).

These experiments will be carried out in the Σ^- hyperon beam with $p_{\Sigma^-} = 2.7$ TeV/c, as well as in the Σ^+ , Σ^0 beams and tagged Λ hyperon ones (produced in the $\Sigma^- \rightarrow \Lambda \pi^-$ decay). Σ^+ and Σ^0 interactions are identified by their final states. As for Σ^+ antihyperons and Σ^- hyperons the experiments will be carried out at the hyperon beam momentum of 2.25 TeV/c and 1.5 TeV/c. Note, that the transitions $\Sigma^{*+} \rightarrow \Sigma^+ \gamma$ and $\Sigma^{*0} \rightarrow \Sigma^0 \gamma$ are forbidden in the SU(3) and SU(6) approximation (by U-spin conservation), and $\Sigma^{*0} \rightarrow \Lambda \gamma$, $\Sigma^{*+} \rightarrow \Sigma^+ \gamma$ are allowed processes. There exists a set of different predictions for radiative widths of hyperon states in the quark model. Therefore the experimental data on the Coulomb production of these particles is of great interest for the spectroscopy of hadrons with light quarks and for the determination of the SU(3) and SU(6) symmetry violation in these hadronic states. Table XI gives the expected statistics for the Coulomb production of some hyperon resonances in the corresponding exposures. The efficient length of the setup in these measurements will be ~ 150 m which would allow one to improve the angular measurement precision and to increase the hyperon decay probability.

4.4. Study of Electromagnetic Formfactors of Unstable Particles

The study of electromagnetic formfactors of unstable particles by their scattering on the atomic electron targets at the momentum transfer $> 1(\text{GeV}/c)^2$ may be realized only at the fixed target machines with the beam energy of > 1 TeV. This scientific program is rather promising for the UNK. It cannot be carried out at the machines with lower energy or at the colliders.

The study of hadron formfactors allows one to check directly the quark counting rule and our notions about quark dynamics on which it is based. Because of the high quality of the UNK hyperon beam the hyperon formfactors may be determined for the first time, which is of great interest from the viewpoint of clarifying the character of the SU(3) symmetry breaking, connected with the s quark becoming heavier. The polarization effects allow one to separate, in principle, the electric and magnetic formfactors of hyperons.

Table II. Detection of Excited Hyperon Production
in the Nucleus Coulomb Field

Reaction	Final state BR	$\sigma_{\text{coul.}}$ $\mu\text{b}/\text{Pb nucl.}$	Hyperon flux/1 s of UNK operation	Number of events per 1 s of UNK operation	Number of events per 10 days of UNK operation
$\Sigma^- + \text{Pb} \rightarrow \Sigma^*(1385)^- + \text{Pb}$ $\downarrow \Lambda \pi^- \rightarrow \rho \pi^- \pi^-$	0.56	~ 1	10^7	~ 20	$6 \cdot 10^6$
$\Sigma^- + \text{Pb} \rightarrow \Sigma^*(1385)^- + \text{Pb}$ $\downarrow \Lambda \pi^- \rightarrow \rho \pi^+ \pi^-$	0.56	~ 30	$1.5 \cdot 10^2$	$\sim 10^{-2}$	$3 \cdot 10^3$
$\Sigma^- + \text{Pb} \rightarrow \Sigma^*(1530)^- + \text{Pb}$ $\downarrow \Sigma^0 \pi^0 \rightarrow \Lambda \pi^0 \pi^0 \rightarrow \rho \pi^- \pi^+ \pi^0$ $\downarrow \Sigma^0 \pi^0 \rightarrow \Lambda \pi^0 \pi^- \rightarrow \rho \pi^+ \pi^- \pi^0$	0.32	~ 0.5	$10^6 + 3 \cdot 10^4$	$0.06 + 0.02$	$(1.8 + 0.6) \cdot 10^4$
$\Lambda + \text{Pb} \rightarrow \Lambda^*(1410) + \text{Pb}$ $\downarrow \Lambda \pi^- \rightarrow \pi^+ \pi^-$ $\downarrow \rho \pi^- \pi^0$ $\downarrow \rho \pi^- \pi^0 \gamma$	0.2 per channel	~ 10	$5 \cdot 10^4 + 1.5 \cdot 10^4$	0.44 + 0.1 per channel	$(1.2 + 0.3) \cdot 10^5$ per channel
$\Lambda + \text{Pb} \rightarrow \Sigma^*(1385)^0 + \text{Pb}$ $\downarrow \Lambda \pi^0$	0.56	~ 30	- " -	3+1	$(9+3) \cdot 10^5$ (nondetectable)
$\Lambda + \text{Pb} \rightarrow \Lambda^*(1520) + \text{Pb}$ $\downarrow \rho \pi^-$	0.23	~ 5	- " -	$0.3 + 0.1$	$(9+3) \cdot 10^4$

- Notes: 1. $\sigma_{\text{coul.}}$ - from M.V.Hynes, Preprint Los Alamos. They may change quite significantly.
 2. Pb target (1.4 g, 0.2 rad.length), i.e., $4 \cdot 10^{21}$ Pb nucl/cm².
 3. Beam momenta $P(\Sigma^-) = 2.7$ TeV/c; $P(\Sigma^*) = 1.5$ TeV/c; $P(\Sigma^-)$ and $P(\Lambda^-) = 2.2$ TeV/c; ± 1.5 TeV/c.
 4. UNK duty factor $\sim 1/3$, i.e., 10 days correspond to effective time of $3 \cdot 10^5$ s.

The following reactions are planned for the study

$$\Sigma^- + e^- \rightarrow \Sigma^- + e^-, \quad (17)$$

$$\Sigma^- + e^- \rightarrow \Sigma^- + e^- \quad (18)$$

at the particle energy of 2-3 TeV. To carry out a comparison with other data obtained at lower energies and for sake of completeness we also plane to have measurements with π mecons:

$$\pi^- + e^- \rightarrow \pi^- + e^-. \quad (19)$$

The cross section for hyperon scattering on electrons (see (17)-(18)) has the form

$$\left[\frac{d\sigma}{d\Omega} \right] = \left[\frac{d\sigma}{d\Omega} \right]_{\text{Mott}} \cdot G_E(q^2)^2 \left\{ \frac{1 + \tau (G_M/G_E)^2}{1 + \tau} + 2\tau \left(\frac{G_M}{G_E} \right)^2 \tan^2 \frac{\nu}{2} \right\}, \quad (20)$$

where $\nu = -t/4M_p^2$; $-t = q^2$; ν is the angle in the coordinate system where electron hits the hyperon at rest.

For proton the electrical and magnetic formfactors have the form $G_E(q^2)_p = G_M(q^2)_p / \mu_p = [1 + q^2/0.71 \text{ (GeV)}^2]^{-2}$. One may also expect the same relation for the Σ^- hyperon: $G_E(q^2)_\Sigma = G_M(q^2)_\Sigma / \mu_\Sigma$; $\mu_\Sigma^- = -1.14 \mu_N$ (μ_p, μ_Σ are magnetic moments). It is convenient to measure the momentum transfer in reactions (17)-(19) by the recoil electron, using the information about its energy: $q^2 = 2m_e E_e \approx 10^{-3} E_e^2 \text{ (GeV}^2\text{)}$.

The characteristic angles for the scattering at $E_\Sigma \approx 2.5 \text{ TeV}$ and $q^2 = 1 \text{ GeV}^2$ are $\nu_\Sigma = 0.4 \text{ mrad}$, $\nu_e = 0.6 \text{ mrad}$, E_e being equal to 1.5 TeV, $E_\Sigma = 1 \text{ TeV}$. The measurements of the electron energy in an electromagnetic calorimeter with an accuracy of $\Delta E/E = \pm 2\%$ yields the accuracy of $\Delta q^2 / q^2 \approx \pm 2\%$. Fig.12 shows the kinematics of reactions (17) and (19). The expected accuracy for the formfactor determination for π mesons and Σ^- hyperons is illustrated in fig.13a and b (in the latter case it is assumed that $G_E(q^2)_\Sigma = G_M(q^2)_\Sigma / \mu_\Sigma^-$).

It is of a special interest to study hyperon resonance production in the reactions

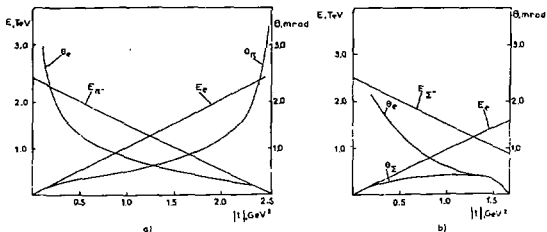


Fig. 12. Kinematics of the reactions $\Sigma e \rightarrow \Sigma e$ and $\pi e \rightarrow \pi e$.

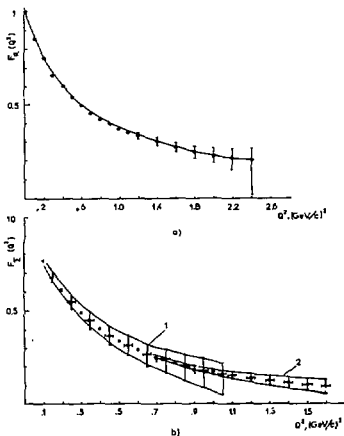


Fig. 13. Expected accuracies for form factor measurements
 a) $F_\pi(q^2)$ (10^7 π/a ; 10 hours); b) $F_{\Sigma^-}(q^2)$ and
 $F_{\Sigma^-\Sigma^+}(q^2)$ (10^7 Σ^-/a ; 100 hours).

$$\Sigma^+ + e^- \rightarrow \Sigma^{*+} + e^-, \quad (21)$$

$$\Sigma^- + e^- \rightarrow \Sigma^{*-} + e^-, \quad (22)$$

$$\Xi^- + e^- \rightarrow \Xi^{*-} + e^-. \quad (23)$$

These reactions will allow one to measure the transition formfactors $Y \rightarrow Y^*$ and to understand the character of the unitary symmetry violation. The transitions of $\Sigma^- \rightarrow \Sigma^{*-}$ type, which are forbidden by SU(3) and SU(6) invariance are of particular interest.

The value for the cross sections at small q^2 is determined by the magnetic moment of the $Y \rightarrow Y^*$ transition $\mu(Y, Y^*)$: $\sigma(Y \rightarrow Y^* + e) \sim \mu^2(Y, Y^*) \sim \Gamma(Y^* \rightarrow Y + \gamma)$. These are just the same processes in the Coulomb field, considered earlier in 4.3. Because of U spin conservation within the limits of the precise SU(6) symmetry the transition moments $\mu(\Sigma^-, \Sigma^{*-})_{SU(6)} = \mu(\Xi^-, \Xi^{*-})_{SU(6)} = 0$, i.e., the cross section of the corresponding processes also turn into zero. However, since SU(6) symmetry is violated by moderate-strong interactions, cross sections (22) and (23) will differ from zero. In ref.[35] total cross section (22) was estimated under certain assumptions on the SU(6) violation mechanism:

$$\sigma \sim \int_{|t_{\min}|}^{|t_{\max}|} |d\sigma/dt| dt \approx 1.1 \cdot 10^{32} \text{ cm}^2. \text{ The dependence}$$

of the SU(6) forbidden transition formfactors on q^2 will be investigated in the reactions on electrons, which is the most interesting, since such data cannot be obtained in the experiments in the nucleus Coulomb field, where q^2 is very small (the condition of coherent interaction with nuclei). The accuracy expected for the $(\Sigma^- \rightarrow \Sigma^{*-})$ vertex transition formfactor in model [35] is shown in fig.13b.

4.5. On Measuring the Σ Hyperon Structure Function.

The study of the Drell-Yan (DY) production mechanism of leptonic pairs in the Σ^- beam allows one to measure the Σ^- hyperon structure function, since the cross section for the relevant process is determined by the quark structure functions of the beam hadrons and the target.

The kinematics of the process is determined by the following quantities:

$$\left. \begin{aligned} M^2 &= x_1 x_2 s, \quad \tau = \frac{M^2}{s} = x_1 x_2, \\ x_F &= x_1 - x_2, \\ x_1 &= \frac{1}{2}(x_F + \sqrt{(x_F^2 + 4\tau)}), \\ x_2 &= \frac{1}{2}(-x_F + \sqrt{(x_F^2 + 4\tau)}). \end{aligned} \right\} \quad (24)$$

The DY pair production cross section [36] has the form

$$\frac{d^2\sigma}{dM^2 dx_F} = K \frac{4\pi\alpha^2}{9sM^2} \frac{1}{x_1 + x_2} \sum_i e_i [q_i^1(x_1) \bar{q}_i^2(x_2) + \bar{q}_i^1(x_1) q_i^2(x_2)], \quad (25)$$

where e_i is the charge of the quark of the i type, $q_i^1(x_1)$ is the probability to find a quark of the i type with momentum fraction x_1 in hadron 1.

The normalization of the quark distributions is as follows

$$\int_0^1 dx [q_i^h(x) - \bar{q}_i^h(x)] = n_i^h$$

n_i^h is the number of valence quarks of the i type in hadron h .

The K factor takes into account the contribution of the higher order QCD corrections. Experimentally $K \approx 1.6$ for pp interactions and $K \approx 2.3$ for meson-proton interactions.

As it clear from (25) the scaling $M^2 \frac{d\sigma}{dM} = F(\tau)$ should take place.

Cross section (25) does not depend on the transverse momentum. However such a dependence was experimentally observed and was established that

$$\langle p_T \rangle = (0.37 + 0.028 \sqrt{s}) \text{ (GeV/c)}.$$

This dependence is explained by the contribution from the processes with gluonic radiation (bremsstrahlung and Compton scattering, see reviews [36,37]).

Intense experimental studies were devoted to the DY production. Table XII presents the main characteristics of the

Table XII. Experimental data on massive lepton pair production

Experiment	Beam		Mass range, (GeV) ($\Delta M/M, \%$)	\sqrt{s} (x_p)	Number of events	$f L dt$ cm^{-2}	Acceptance %
	Types of particle and their E	Intensity, (s^{-1})					
OFS/38/	p (200,300, 400)	$\sim 10^{12}$	4-18 (2%)	0.15 ± 0.65 ($-0.1 < x_p < 0.4$)	10^6	$\sim 10^{42}$	0.5
MNTW/39/	p (400)	$2 \cdot 10^{11}$	6-16 (7.5%)	0.22 ± 0.58 ($x_p > -0.2$)	$2.25 \cdot 10^5$	$\sim 4 \cdot 10^{41}$	5
NA3/40/	π^- (280)	$\sim 10^7$	4.2-8.5	0.18 ± 0.37	$1.2 \cdot 10^4$	$2.8 \cdot 10^{38}$	10±30
	p (400)	$1.5 \cdot 10^9$	4.5-8.5 (4.5%)	0.16 ± 0.31 ($x_p > -0.31$)	$3.0 \cdot 10^4$	$4 \cdot 10^{39}$	
NA10/41/	π^- (194)	$2 \cdot 10^9$	4.1-15 (3%)	0.21 ± 0.17 ($x_p > -0.2$)	$1.58 \cdot 10^5$	$1.6 \cdot 10^{40}$	~ 5
CHPMNP/42/	p+p (ISR) $\sqrt{s}=62$ GeV		2-25	0.03 ± 0.40	$1.4 \cdot 10^4$	$1.1 \cdot 10^{38}$	~ 2.5
			5-8 (10%)	0.08 ± 0.13 ($-0.1 < x_p < 0.5$)	$4.4 \cdot 10^3$		
UNK hyperon experiment	Σ^- (2800)	$\sim 2 \cdot 10^7$	2-25	0.03 ± 0.35	$4 \cdot 10^5$	$3.5 \cdot 10^{38}$	~ 20 ($M > 4$ GeV)
			4-25	0.06 ± 0.35 ($x_p > -0.1$)	$3.5 \cdot 10^4$		

dimuonic experiments with largest statistics and at maximum energies.

The estimates of the DY pair production cross sections in Σ^- W-interactions obtained in accordance with (25) (K=1) and with known nucleon structure functions under assumption on the SU(3) symmetry for Σ^- , are presented in Table XIII and at fig.14.

Table XIII. Statistic of massive lepton pair production in Σ^- N interactions.

M (GeV)	$\tau=M^2/E$	σ (DY) nb/nucleon	events/ 10 days	Number of events/sec
2-2,8	0.03-0.04	4.0	$2.7 \cdot 10^5$	0.9
2,8-4 (ψ region)	0.04-0.06	1.36	$0.9 \cdot 10^5$	0.3
4-9	0.06-0.12	0.476	$3 \cdot 10^4$	0.1
9-11 (Υ region)	0.12-0.15	0.010	$7 \cdot 10^3$	$2.3 \cdot 10^{-3}$
11-15	0.15-0.21	$4.8 \cdot 10^{-3}$	$3 \cdot 10^2$	$1 \cdot 10^{-3}$
15-20	0.21-0.28	$0.8 \cdot 10^{-3}$	55	$2 \cdot 10^{-4}$
20-25	0.26-0.35	$116 \cdot 10^{-6}$	~ 10	$26 \cdot 10^{-6}$
25-35	0.35-0.48	$21 \cdot 10^{-6}$	~ 1	$5 \cdot 10^{-6}$
4-25	0.06-0.35	0.49	$\sim 4 \cdot 10^4$	0.104

- Notes: 1. A W target 5 cm thick (97 g/cm^2) will be used in the experiment;
2. The Σ^- hyperon flux during the measurement period (10 days) will be $I=6 \cdot 10^{12} \Sigma^- (2 \cdot 10^7 \text{ E}^-/\text{sec}^{-1})$, the UNK accelerator duty-factor 1/3). The integral luminosity in the experiment will be $L=7 \cdot 10^{37} \text{ cm}^2$ (with an account of the 20% detection efficiency for $\mu^+\mu^-$ pairs at $M_{\mu^+\mu^-} > 4 \text{ GeV}$);
3. In calculations of the muon pair yields no account was made of the K factor.
4. The background from semileptonic decays of B-mesons for $M_{\mu^+\mu^-} > 4 \text{ GeV}$ is $< 2\%$ of events.

The results of calculations agree with the scaling extrapolation of the ISR data according to

$$\frac{d\sigma}{dW} = \frac{A(1-\sqrt{\tau})^{10}}{W^3\sqrt{\tau}} \quad (26)$$

The study of the DY pair production for $\sqrt{\tau} > 0.06$ using the statistics of ~ 35000 events will make it possible to reconstruct the structure function of Σ^- -hyperons in the range $0.06 < \tau < 0.6$ and to compare it with the data on the proton structure function obtained in a special exposure with a proton beam ($E_p \sim 3$ TeV). The results of comparing the data obtained in one experiment, will be free from a number of systematic uncertainties.

It is assumed that in this experiment the W target and the system for measuring the muon emission angles (hodoscope detectors, microstrip detectors) will be installed in front of the first magnet. Then there will be a beam-dump $\sim 6-7$ m long (partially in the first magnet). Muon pairs will be detected in the second magnetic spectrometer. Trigger should select the pairs with $W > 4$ GeV.

4.6. Study of Weak Hyperon Decays

Good quality of the UNK hyperon beams allows one to use them for high precision studies of weak hyperon decays and search for rare processes of this type. The sensitivity of the relevant experiments may be 10^{-13} for Σ^- decays, 10^{-11} for the Σ^- and Λ^0 decays, and 10^{-8} for α^- decays (the decay $\Sigma^- \rightarrow \Lambda^0 \pi^-$ is the source of the tagged polarized Λ^0 hyperons).

As the examples of such rare processes which require high sensitivity, we may take the decay

$$\Sigma^- \rightarrow \Lambda e \bar{\nu} \quad (27)$$

(its relative probability is $5.7 \cdot 10^{-5}$) as well as anomalous decays with $\Delta S=2$ (e.g., $\Sigma^- \rightarrow p \bar{\pi}^- \bar{\pi}^-$). Let us consider process (27) in more detail.

The maximum length of the setup should be used in the experiments with cascade hyperon decays, since the Λ hyperon detection efficiency improved greatly with the increase of the effective decay path (see fig.15). The kinematics of decay (27) is presented in Table XIV.

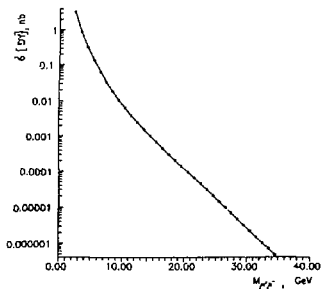


Fig. 14. The Drell-Yan muon pair spectrum in the reaction $\Sigma^- + N \rightarrow (\mu^+ \mu^-) + X$.

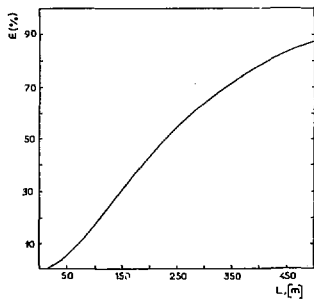


Fig. 15. The $\Sigma \rightarrow \Lambda e \nu$ decay: the dependence of the detection efficiency on the decay path length, where the Λ hyperon decays are detected.

Table XIV Kinematics of the $\Sigma^- \rightarrow \Lambda e^- \nu$ decay (at $P_{\Sigma^-} = 2700$ GeV/c)

Particle	E_{\min} (GeV)	E_{\max} (GeV)	$\langle E \rangle$	Maximum angle (for $\langle E \rangle$)
Λ	2340	2700	2520	$3.2 \cdot 10^{-5}$
e	0	180	360	$4.4 \cdot 10^{-4}$
p	1900	2130	2360	$4.7 \cdot 10^{-5}$
π^-				

The accuracy of the corresponding measurement angles should be 10^{-6} . Maximum transverse dimensions of the facility with the common length of $L \approx 200$ m is 80 cm and are mainly determined by the initial hyperon beam divergences. A magnet spectrometer based on the magnet M3 is planned to be used. The statistics of 10^7 decays (2T) may be acquired per 1 day of measurement.

5. MAIN ELEMENTS OF THE EXPERIMENTAL SETUP

5.1. Hyperon beam identification system

The hyperon beam identification system is designed for incident particle identification and to determine its trajectories with a $3 \mu\text{m}$ accuracy along x - and y - axes. The facility includes hodoscopes, scintillation counters, silicon microstrip detectors SSDI with a $20 \mu\text{m}$ step and transition radiation detectors. At $\sigma_x; \sigma_y \approx 3 \mu\text{m}$ and path length of about 2m the error in determining the incident hyperon angle is $3 \cdot 10^{-3}$ mrad, which corresponds to the a possible contribution of $\delta t < 10^{-4}$ (GeV/c) 2 . At the particle flux of $> 10^7/\text{s}$, uniformly distributed over a 0.5 cm^2 spot, the SSD life-time will be 0.5 year. This problem needs a thorough experimental study.

To identify the primary beam particles (mainly for π meson impurity suppression) we use the transition radiation detector, which can quite efficiently separate hyperons and pions because of a great difference in their Lorentz factors ($1+2 \cdot 10^4$). The charge accumulation in such a detector may be < 100 ns. The separation of the Σ hyperon and π meson transition radiation at 1.5, 2.5 and 2.7 TeV is shown in fig.16.

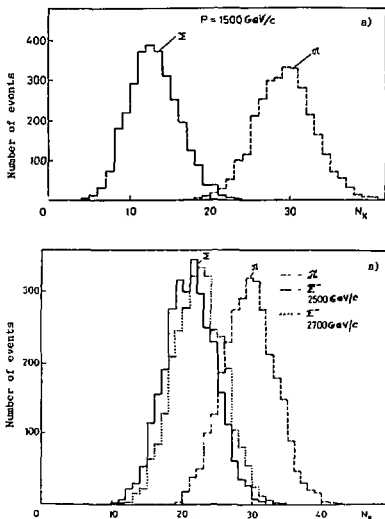


Fig. 16. Separation of Σ mesons and Σ hyperons of the primary beam using the transition radiation detector TRD-1: a) $P=1500 \text{ GeV}/c$; b) $P=2500 \text{ GeV}/c$ and $P=2700 \text{ GeV}/c$.

In the case of necessity the hyperon beam momentum may also be measured with a 1% accuracy with the help of the last purifying magnet in the system of hyperon beam formation (see Ch. 2).

5.2. Vertex detector

The study of the short lived beauty particles requires a detector which has high spatial resolution ($<20 \mu$), fast response and would be capable to work with high multiplicities. The charmed and beauty particles produced in the target decay, after covering a short path, yielding one or more secondary vertices with the increase of the particle number. One of the main tasks of the vertex detector is to detect heavy particles secondary decay vertices. This is one of most important criteria for the selection of the events with beauty particles, whose fraction is $\sim 10^{-5}$ from the total number of the events. The vertex detector should have a high efficiency for particle detection. The thickness of the vertex detector should be minimal to reduce the multiple scattering, photon conversion and secondary particle interactions. The detector should be able to work under hard radiative conditions, caused mainly by the passing of the primary beam.

At present we are considering different variants of the vertex detectors based on the microstrip detectors (MSD), scintillation fibers and charge coupling devices (CCD) in combination with MSD. The final choice of the vertex detector will be made after a completion of investigations. Quite possibly the detector will include a combination of several types of precise devices, which may greatly simplify the construction of electronics and improve the detector characteristics. This section is devoted to the consideration of a vertex detector based on microstrip detectors. All other variants are given in Appendix III and Appendix IV.

The proposed vertex detector (VD) (see fig.17) incorporates twelve MSD stations installed along the beam at a distance of 20 mm from each other. The vertex detector length is 250 mm. Its transverse dimensions are determined by the beam sizes and angular acceptance of the facility (± 0.1 rad) and

varies from $(15 \times 15) \text{ mm}^2$ in the first station up to $(45 \times 45) \text{ mm}^2$ in the end stations, starting from station 7.

The first six stations of the vertex detector make up an "active target", where the primary interaction takes place. The remaining six coordinate stations are used for the determination of the charged particle tracks.

The active target station consists of four planes of one-sided MSD (X, Y, X', Y'), each $300 \mu\text{m}$ thick with $25 \mu\text{m}$ strips, and 1 mm thick silicon ΔE detector. The MSD planes are installed symmetrically with the w. r. t. ΔE detectors and serve to point to the coordinates of the charged particle tracks, while the ΔE detector provides the information about the changes in the number of charged particles, hitting the detector area. The active target total thickness is 0.345 nuclear length and 0.2 radiation length. The choice of the target thickness was determined from the requirement for the sufficient number of interactions of incident beam particles at an acceptable level of photon conversion. The active target stations are distributed along the beam to localize secondary vertices from beauty particles outside the target matter. The active target design envisages a possibility to increase the target thickness and to study the dependence of the production cross section of beauty particles on the atomic number of proper insertions.

The coordinate station consists of two two-sided MSDs (X, Y, X', Y') $200 \mu\text{m}$ thick each with $25 \mu\text{m}$ strips. The sixth and seventh coordinate stations contain also ΔE detectors $300 \mu\text{m}$ thick which provide information about the changes of the number of charged secondaries in the events caused by decays of beauty particles, produced in the end station of active target.

The MSDs will be manufactured from the plates of high resistance silicon of the n type, 200 and $300 \mu\text{m}$ thick, onto which the strips will be put with planar technology. With the $25 \mu\text{m}$ step the strip width will be $10 \mu\text{m}$. The maximal dimensions of the sensitive area will be $45 \times 45 \text{ mm}^2$. The efficiency of detecting one minimal ionizing particle (MIP) is expected to be 99.99% . The MIP energy losses in silicon is $26 \text{ KeV}/100 \mu\text{m}$, which corresponds to the production of 25000 pairs of carriers in $300 \mu\text{m}$ of MSD. The signal-to-noise ratio will be (10 ± 20) . The

spatial accuracy is expected to be $< 5 \mu\text{m}$ when averaging over a cluster (determined over one strip $25/\sqrt{12} = 7.2 \mu\text{m}$). The average size of the cluster is 1.6 strips, the hitting probability for one or two strips is 95%. The resolution between two tracks is $100\text{--}150 \mu\text{m}$, which corresponds to the angular resolution $(0.4\text{--}0.6) \cdot 10^{-3}$ mrad. As it follows from the estimations, the information from the six stations allows one to reconstruct the vertex of the B particle decay with an accuracy of $10 \mu\text{m}$ in the plane transverse to the beam and of $100 \mu\text{m}$ along the beam.

The detector which would meet the requirements of experiment, should, from the very beginning, have not less than 99% of the strips with the leakage current < 10 nA. During the experiment with the beam the leakage current should not exceed 200 nA. With this value exceeded the contribution from the noises becomes significant.

The charge collection time for the MSD $300 \mu\text{m}$ thick is 10 ns. This allows one to include the vertex detector into the trigger.

The number of MSDs in the vertex detector is equal to 36 with the total number of the information channels $3 \cdot 10^6$, which can be reduced by 30-40% if the vertex detector configuration is changed.

The vertex detector design should allow for geometry changes, access to certain stations, replacement of the target material, fine adjustment and control of the target and MSD position. The strategy of assembling the vertex detector foresees the adjustment of the stations with an accuracy up to tens of μm in combination with a high mechanical stability of the whole vertex detector structure ($5 \mu\text{m}$) and high accuracy of controlling their position in space ($2 \mu\text{m}$). The accuracy for the relative position of the strips in the MSD, for gaps, and strip sizes over the area of the detector is $1 \mu\text{m}$, which is guaranteed by the photolithography process used in industry. The MSD adjustment will be carried out with optical method when assembling the detectors: the position of the MSD planes will be measured respect to the fiducial points of the stations. The relative position of the stations will be then determined using geodesic and optical techniques over the reference points in the course of the vertex detector assembling and with further precise measurements using the particle beam and collimated X-ray beam. The radiati-

ve stability of MSD when irradiated by the photons from the Co^{60} source, is estimated to be $2 \cdot 10^6$ rad and being irradiated by relativistic particle fluxes $\sim 10^5 + 10^6$ rad, which corresponds to the integral fluxes of $10^{13} + 10^{14}$ p/cm². This problem is being intensely studied now.

5.3. System of fiber track detectors

The track system for particle detection upstream of the first magnet spectrometer will be supplemented by a system of the scintillation fiber detectors. The detectors of this type are considered in detail in Appendix 3. The track fiber system will be installed after the vertex detector. The system includes seven planes of fiber glass with the read out on one CCD (596-1088 cells). Three planes are installed right after the vertex detector (X, Y, V), two planes are at a distance of 15 cm from the vertex detector and two planes (X,Y) are at a distance of 30 cm*. The planes consist of capillaries 50 cm long with the inner diameter 150 μ m and outer - 200 μ m, each plane is 1.5 mm thick along the beam. The plane sizes are chosen such as to cover the polar angle of ± 100 mrad. The smallest transverse size of the planes is 50 mm and the largest one is 90 mm. The planes are connected to the photocathode image intensifier (II) with the diameter of 50 mm. The total number of the fibers is $1.5 \cdot 10^4$, the total length of 7 km.

The fibers from all the planes are read out by one intensifier system (three II, one CCD). The image reduction factor is $K_{red} = 8$. Along the distance $L = 50$ cm and the plane 1.5 mm thick the number of photoelectrons is $N \sim 10$.

The space resolution σ_v mainly depends on the fiber sizes. For the diameter 150 μ m $\sigma_v \approx 50$ μ m. The contribution from the cell sizes ($15 \times 15 \mu$ m²) $\sigma_{CCD} = 15 K_{red} / \sqrt{2} = 34.5$ μ m. All the other contributions may be negligible: $\sigma = \sqrt{\sigma_v^2 + \sigma_{CCD}^2} = 60$ μ m. The accuracy of the track localization is

* If a Cerenkov detector RICH¹ (as is shown in fig.3) be put in front of M1, the structure of the detector may somewhat change. Several fast response proportional chambers, manufactured lithographically, may also be used.

$$e = \frac{\sigma}{2} \sqrt{\frac{12N}{(N+1)(N+2)}} = 29 \mu\text{m}.$$

The accuracy is $\delta \approx 35 \mu\text{m}$ with an account of the multiple scattering. The error in determining the angle (along the 30 cm path length) is $\sigma_{\theta} \sim 10^{-4}$.

The resolution between the tracks is determined by II and CGD cell sizes and is equal to $\Delta < 200 \mu\text{m}$.

At present the time resolution is 150 ns (see Appendix III). The application of optoelectronic delays will allow one to obtain the time resolution of < 10 ns.

Dead time is determined by the time of transfer, readout and a possibility to buffer the data in CGD. The information transfer from the accumulation section to the memory section of the CGD takes 30 μs , the readout time is 350 μs . The scintillation fiber image occupies a small area in CGD therefore one has a possibility of buffering for five events.

5.4. Track system

The track system of the facility consists of four blocks of minidrift chambers DG1, DG2, DG3, DG4 (see fig.3).

Each block consists of four modules with identical structures: XYUV. Each plane (X, Y, U, V) is doubled. Consequently each block has 16 doubled planes (to avoid left-right uncertainty). The chamber sizes, the width of drift cells and the number of channels are given in Table V.

5.5. Secondary particle identification

Ring image Cerenkov detectors (RICH) and transition radiation detectors (TRD), whose location within the setup layout is shown in fig.3, are used for secondary particle identification.

5.5.1. Ring Image Cerenkov Counters

The requirements imposed on the multichannel differential Cerenkov counters assigned for the identification of secondary charged particles, are as follow

- good time resolution (< 10 - 20 ns);
- capability to work at high intensities ($> 1+2 \cdot 10^7$ pps) and to detect events with charge multiplicity up to 30;

- high detection efficiency (>95%);
- stability and reliability in operation.

Since the duration of the Cerenkov light radiation ($<10^{-11}$ s) is considerably less than the duration of the signals from the photocathode used in the Cerenkov devices, all the requirements imposed on the RICH counters are true for PMS or gas photoionization chambers.

There exist new designs of photoionization chambers with time resolution of 15-20 ns (Parallel-Plate Avalanche Chamber with pad anodes and MWPC type with pad cathode) to be used in high intensity particle beams. Because of the difficulties in manufacturing and exploitation of large chambers with such electronics, we propose to use small-sized or multianode PMS for the Cerenkov ring detection. Photosensitive walls of several square meters may be composed of these PMS which will satisfy all the requirements imposed on the RICH counters.

The prototype of such a multichannel Cerenkov spectrometer, now operating as a component of the SPHINX facility, was constructed at IHEP in 1989.

The principal optical scheme of this detector is shown in fig.18. A 736 channel photosensitive system was used to detect Cerenkov radiation. PM-60 with the bulb diameter 15 mm and amplification factor of $>10^5$ were used as photodetectors. PM glass photocathodes were covered with shifter to increase the yield of photoelectrons from Cerenkov radiation. The electronics provided the amplification required for a reliable detection of one-electron signals from the PM. The results obtained from preliminary processing showed high efficiency and almost complete absence of the background. A multiparticle event in this Cerenkov counter is shown as an example in fig.19. The results obtained with the prototype detector showed that PM-60 may be used for the Cerenkov spectrometers at the UNK as well.

Three RICH counters, which allow to identify π, K and p in the momentum range up to 200 GeV/c, will be used in the facility for hyperon studies (see fig.3). For particle identification at higher momenta TRD detectors can be used.

The first RICH detector with the radiator length of about 1 and a relatively small number of channels will be installed between the vertex detector and the magnet M1. It will be

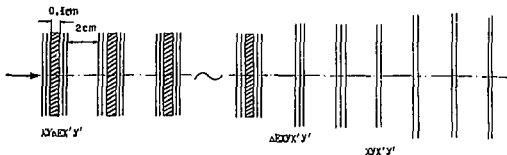


Fig. 17. The layout of the active target and the vertex detector with microstrip silicon registers and silicon semiconductor counters ΔE for ionization measurements.

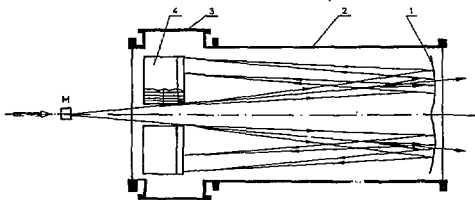


Fig. 18. The layout of the 736-channel detector RICH, used as a component of the SPRINK facility for the detection of secondary particles. 1 - spherical mirror of thin glass ($\Delta=5\text{mm}$, $f=125\text{mm}$); 2 - detector body; 3 - flanges of the output plugs; 4 - a set of the PMs (each of two sets contains 368 PM 60).

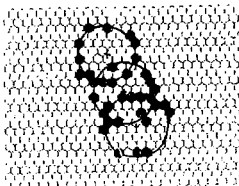


Fig. 19. Multiparticle event, detected in RICH at SPRINK. Three Čerenkov rings are singled out

used for the identification of particles with momentum up to 30 GeV/c and emission angle $>15-20$ mrad. The second RICH detector with the radiator 5-6 m long is installed between the magnets M1 and M2, to identify particles with momenta up to 100 GeV/c and emission angle up to ± 75 mrad (this angular range was chosen with an account of the deviation of particles in the magnetic field of M1 and emission angles of particles from hyperon decays). RICH 3 counter with the radiator 15 m long will be installed after the magnet M2 will to cover the momentum range up to the region where secondary particles will reliably be identified with the TRD detectors.

The main calculated characteristics RICH1, RICH2 and RICH3 detectors are given in Table XV.

5.5.2. Transition radiation detectors

It is planned to use several transition radiation detectors for the identification of beam particles, electrons from the secondary particle decays and for separation of π and K mesons with the γ factor $>10^3$ in the region where their identification by Cerenkov radiation is complicated.

The beam identifier TRD1 serves to separate hyperons and π mesons in the primary beam at $E > 1.5$ TeV. TRD1 consists of 20 modules, each module contains a radiator and 3-sectioned proportional chamber. The radiator, consists of 200 layers of polypropylene film $17 \mu\text{m}$ thick with a 0.5 mm gap and the area of $2 \times 2 \text{ cm}^2$. The proportional chamber with 0.5 mm step was filled with xenon-methane (30%) mixture. The separation of π and Σ hyperons at 1.5, 2.5 and 2.7 TeV is shown in fig.16.

TRD2, installed after the RICH2 counter (see fig.3 and Table V), is $2 \times 1.5 \text{ m}^2$ and 5 modules. Each module contains a polypropylene radiator and proportional chambers with 3 mm pitch. The number of channels in this detector is 6000. π -meson rejection was 10^3 at 90% detection efficiency for electrons.

TRD3 is also used for electron selection and is equivalent to TRD2 in its structure.

TRD4 separates π and K mesons with energies higher than 150 GeV. There are 10 modules $3 \times 2 \text{ m}^2$, each module containing a radiator of propylene film layers and (X,Y) proportional chambers with 3 mm step, respectively. The number of de-

tection channels in the chambers is $1.7 \cdot 10^4$. At 90% efficiency of π meson detection the K meson rejection depends on the particle momentum and varies from 10^3 to 10 in the momentum range from 150 up to 1500 GeV/c.

Table XV. Characteristics of Multichannel Cerenkov Spectrometers of the RICH Type.

	RICH-1	RICH-2	RICH-3
Focusing distance of spherical mirror (m)	1.5	6.0	15.0
Radiator length (m)	1.0	5.0	15.0
Radiator gas;	Freon 12	CF ₄	Ne
refraction coefficient			
$(n-1) \cdot 10^6$	1012	470	64
Spherical mirror sizes (m ²)	ϕ 0.5	(2.1 \times 2)	2.7 \times 2.5
$P_{\text{thres.}}$ (GeV/c)			
$\pi/K/p$	3.2/11.5/23	5/18/36	13/46/92
ΔR (disp) (mm) (FWHM)	3	5	3.75
R_{max} (mm)	68	163	165.8
$n_{\text{fe}} (\beta=1) = 100 \theta^2 L$ (cm) G.B	16.5	36	15
$(\Delta\beta/\beta)_{\text{ideal}}$ (FWHM) = $= \text{tg} \theta \Delta\theta / \sqrt{n_{\text{fe}}}$	$2 \cdot 10^{-6}$	$4 \cdot 10^{-6}$	$7.5 \cdot 10^{-7}$
Assumed angular range (mrad)	± 100	± 75	± 30
The area of photodetector (m ²)	0.5 \times 0.5	1.1 \times 1.1	1.1 \times 1.1
Number of PM -60	10 ³	5 \times 10 ³	5 \times 10 ³
ΔR (for PM -60) = $= 15 / \sqrt{12} n_{\text{fe}}$ (mm, FWHM)	2.5	1.7	2.7
$\Delta\beta/\beta$ (FWHM)	$8 \cdot 10^{-5}$	$8 \cdot 10^{-6}$	$2 \cdot 10^{-6}$
The ultimate momentum for particle separation			
$P_{\pi/K}$ (GeV/c),	35	100	240
$P_{K/p}$ (GeV/c)	60	180	400

5.6. Triggering logic.

The main problem in the study of the particles with heavy quarks in hadron collisions is to suppress the background from the ordinary interactions, whose cross section is 10^5 times larger than for the processes with beauty particles production.

Recording of about 1 Mb of information per second on tape seems to be quite realistic, which makes up to 50 events at the average event length of 20-25 Kb.

The triggering system should have a multilevel structure to provide such selection factor.

All the calculations for the system are given for the primary beam intensity of $2 \cdot 10^7$ pps and target 0.05 interaction length thick. Numerical estimations for the selection factors were Monte-Carlo calculated with the help of the LUND and ISAJET programs. The following scheme for the triggering logics is planned.

The first level trigger fixes the interactions with the target (rejection ~ 20) and the requirement higher multiplicity in the events with heavy particles (selection coefficient 2). As the calculations have shown, the number of charged particles in the $b\bar{b}$ pair production is, in average, by 10-20 larger than in the soft processes. The decision time is 15 ns. The output flux will be $5 \cdot 10^5$ events/sec, and beam losses are 30%.

The trigger of the second level is based on a jump of charged particle multiplicity, which arises from the decay of particles containing b quarks. Using the information from the ΔE detector one can suppress the event flux ten times during 80 ns. The output flux will be $5 \cdot 10^4$ events, the dead time being 4%. This can be seen from the calculations given in figs.20 and 21. The second level trigger initiates the readout of the information from the registers to the buffer memory.

As is known the particles with b quarks are produced in hard collisions with large transverse momenta ($\langle p_T \rangle > 2.8$ GeV/c) contrary to the soft processes ($\langle p_T \rangle \sim 0.35$ GeV/c). Besides, in their decays there are produced particles with large p_T . Therefore the third level trigger analyses the transverse energy of the particles produced using the information from the calorimeters. Moreover the decay products of b particle occur in some interval over pseudorapidities. Hence, the selection of events

over the total value for the transverse energy in a certain range of pseudorapidity may yield this or other degree of the rejection at a given efficiency of b particle detection.

Fig.22 shows the dependence of the detection efficiency for b particle on the degree of the background rejection (upper curve), the information about the total transverse energy within the rapidity interval of $3.2 < \eta < 5.2$ from the calorimeters being used. The lower curve shows the dependence of the rejection on the cutoff value, imposed on the total transverse energy (left scale).

The decision time is $1 \mu s$, the rejection factor is 10 at the detection efficiency $> 50\%$. The output flux will be $5 \cdot 10^3$ events/s at 5% dead time.

The follow trigger processors work with bufferized information.

The fourth level trigger recognizes the presence of the tracks, not directed to the primary vertex. A vertex detector being used for this purpose. The idea that was checked in the the simulation, consists in:

- first the coordinates of the primary vertex inside one of the six target stations were determined with a special procedure;
- then, in each X_i and Y_i plane of the station, right after the target station, the number of hits was determined: $N = N_1 - N_2$, where N_1 is the total number of hits in a given i-th plane of the station, and N_2 is the number of hits belonging (in the given error bars) to the straight lines passing through the primary vertex and corresponding hits of the subsequent (i+1) or (i+2) stations.

The N distribution histograms for the events with B particles are presented in fig.23b, and fig.23a - for the background events.

Fig.24 presents the selection efficiency for the events with B particles obtained with the help of these histograms, as a function of the rejection factor of background events (for different values of the error bars).

From the calculations it follows that one may achieve the rejection factor of 10 at the B particle detection efficiency of $> 50\%$.

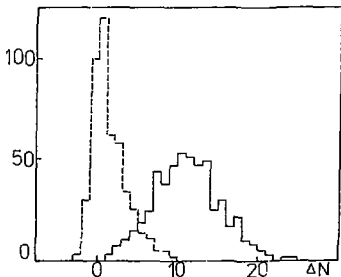


Fig. 20.
Charge particle multiplicity jump in the interactions with an active target: broken line - "soft" events", solid line events with $b\bar{b}$ production.

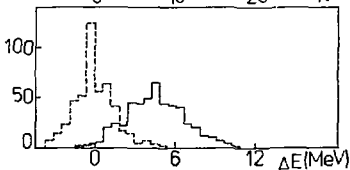


Fig. 21.
Charge jump in the interaction with an active target: broken line - "so" events", solid line - events with $b\bar{b}$ production.

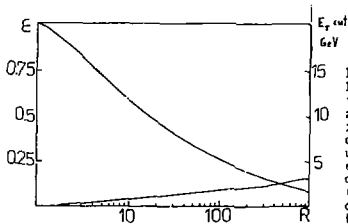


Fig. 22.
Detection efficiency for the particles with b quark versus the background rejection with application of the information about summed transverse energy in the pseudorapidity range of $3.2 < \eta < 5.2$ (upper curve). Lower curve and the scale on the right: the dependence of the background rejection on the cut over F_T .

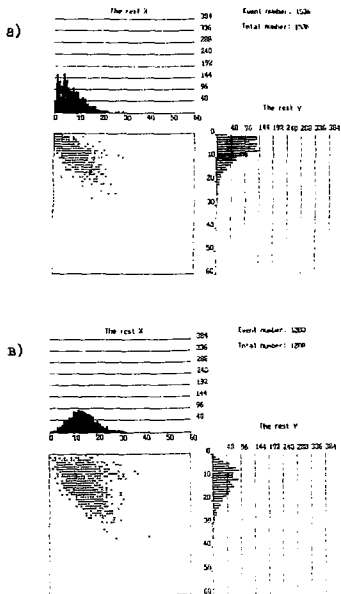


Fig. 23. The number of "hits" in the microstrips of the X and Y planes, the nearest to the interaction vertex, remaining after "hits" subtraction for the tracks, coming from the primary vertex: a) for "soft" events; b) for the events with $b\bar{b}$ production.

The decision time is 100 μ s, the output flux is 500 events/s. At the fifth level of the trigger the reconstruction of the events in the vertex detector takes place and the number of secondary vertices is determined. During 10 μ s one can achieve the selection factor of 15 and make the data flux 30-40 events/s. In principle, other selection techniques for useful events may be used, for example, by detecting leptons with large transverse momenta (see fig.25).

Table XVI shows the above quoted data on the system of organizing a trigger for the selection of beauty particles.

5.7. Data acquisition system (see also Appendix 5)

The electronics should be realized in the FASTBUS standard, maybe using a simplified protocol.

The information readout time in the FASTBUS crate (the size of the event 20-25 Kb) is approximately equal to 10 μ s. The events are to be read out in average each 200 μ s. Therefore the information should preliminary be buffered in the receiving registers, containing a buffer for 2-6 events so as to maintain the dead time at an acceptable level. The information from the FASTBUS registers is then recorded in the preliminary buffer memory (4-10 events) assembled in each crate with front-end electronics. Then specialized processors are put into operation, repacking the accepted event and making partial conversion of the information. So as they may also calculate some sums (with the weights included) all these will then be used in trigger and record the data into the buffers of Event Builder devices. Some events may be put into the buffers without any conservation. The buffers are grouped according to the types and of the devices (e.g., over the X, Y projections in the dtif chamber blocks, etc.).

This information is used for the next level trigger production. Specialized processors, used for trigger decision allow one to reduce the information down to 50 events per second. Selected events are the inputs for the universal microprocessors (micro-processor farm). Their goal is a complete processing of the data, final selection of the events of the required class, forwarding and packing the information. The total power required for the solution of all these problems is about 100 MWPS.

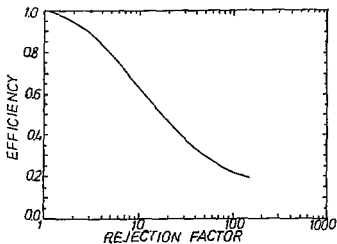


Fig. 24. Detection efficiency for the events with the production of particles with $b\bar{b}$ quarks versus the background rejection using the selection criteria over the "hit" differences in the vertex detector planes (see fig.23 and the text).

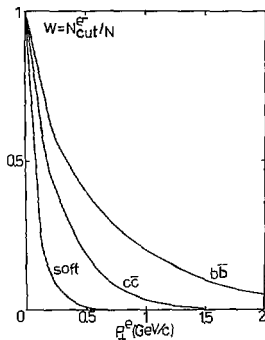


Fig. 25. The selection of the events with the $b\bar{b}$ production when detecting leptons with large transverse momentum.

Table XVI. Block diagram of trigger signal forming.

	Input flux (events/s)		Decision time	Rejection	Dead time %
1	2×10^7	Interactions with higher multiplicity	15 ns	40	30
2	5×10^5	Multiplicity jump (detectors dE/dx)	80 ns	10	4
3	5×10^4	Large transverse energy	<1 μ s	10	5
4	5×10^3	Counts of the hits from the tracks some secondary vertices	100 μ s	10	5
5	5×10^2	Determination of the number of secondary vertices	10 ms	15	1

40 ÷ 50 events/s: writing on magnetic tape ~1 Mbyte/s

One of the possible versions is the application of the processor farm the ACP type (FNAL), consisting of 10 blocks with the power up to 20 MIPS. One of the blocks is to work as an Event Builder and besides it should record the information on tape.

The resulting output flux will be ~50 selected events per second, or about 1-2 Mb per second. To manage such flux one may use 2-3 devices of the EXABYTE type (in parallel), i.e., all in all one needs 6 devices of this type. The higher the response of these devices the less in their number.

A multi-user computer with the processor of the same type as in the microprocessor farm seems to be expedient in this case, though a computer of the MicroVAX type may also be acceptable.

Sufficiently cheap Equipment computers with a direct access to the front-end electronics are to be used for the test and control the apparatus.

The experimentators should be supplied with a set of 32-bit personal computers operating together with the main computer and Equipment computers.

A set of special-purpose microcomputers should be used to control the power, gas supply systems as well as some other elements of set up.

Table XVII. Some types of exotic hadrons with heavy quarks

Type of exotic particles	Notations	Quark composition	Main characteristics	Decay channels
1	2	3	4	5
1. Open exotic strange-charmed mesons (with an exotic set of quantum numbers $I;S;C$ [23]).	\tilde{F}_u^0	$os\bar{u}$	$(I;S;C)=0;-1;+1$	$\tilde{F}_u^0 \rightarrow D^+ K^- - K^+ K^- \pi^+ \pi^+$ If the meson mass below the DK threshold then a weak decay $\tilde{F}_u^0 \rightarrow K^+ K^- \pi^+ \pi^+$ take place
	\tilde{F}_I^{++}		$(I;S;C)=1,1,1$	$\tilde{F}_I^{++} \rightarrow D^+ K^+; D_s^+ \pi^+$
	\tilde{F}_I^+ \tilde{F}_I^0	$o\bar{s}(q\bar{q})_{I=1}$	$(I;S;C)=1,1,1$ $(I;S;C)=1,1,1$	$\tilde{F}_I^0 \rightarrow D^0 K^0; D_s^+ \pi^-$ $\tilde{F}_I^+ \rightarrow D^+ K^0; D_s^+ \pi^0$
Cryptoexotic mesons of this type [23]	F_X^+	$o\bar{s}(q\bar{q})_{I=0}$	$(I;S;C)=0,1,1$	Electr. mag. decays: $F_X^+ \rightarrow D_s^+ \pi^+ + 2\gamma;$ $D_s^+ \pi^0; D_s^+ \pi^0 \gamma$ (if $F_X^+ \notin DK$)
Open exotic mesons with two heavy quarks: $Q=b; c$.		$(Q^2\bar{q}^2)$	$B=2$ OR $\{B=1$ $C=1$ etc.	The lightest state (the $bb\bar{u}\bar{d}$), ($bb\bar{u}\bar{d}$) type should be stable respect of strong and electromagnetic interactions (from QCD analysis).

Table XVI (continued)

1	2	3	4	5
2. Strange-anti-charmed baryons with exotic quantum numbers [24]	P_c^0 $\bar{c}s$	$(\bar{c}uds)$	$(I;S;C)=$ $=1/2;-1;-1$	$P_c^0 \rightarrow p\bar{p}\bar{c}; p\bar{p}\pi^-; AK^0\pi^0$ (weak decays). With a large probability these states are stable respect to strong and electromagnetic interactions.
	P_c^- $\bar{c}s$	$(\bar{c}uds)$		$P_c^- \rightarrow \Sigma^-\bar{c}; K^0K^0P$ (weak decays). These states may be stable w.r.t. strong and electromagnetic interaction
	P_c^+	$(\bar{c}uds)$	$(I;S;C)=0,-2,-1$	
	$P_c^0; -; -; -$ (I=1)	$(\bar{c}qqqs)$	$(I;S;C)=1,-2,-1$	
3. Similar states with b-quarks		$(\bar{b}qqqs)$ $(\bar{b}qqqs)$		
4. Quasixotic mesons with hidden charm (4-quark mesons and hybrids)	$M_{\psi}^{(1)}$	$[\bar{c}\bar{c}(q\bar{q})_{I=1}]$	$I=1 \quad S=C=0$	$M_{\psi}^{(1)} \rightarrow \psi\eta; \psi\rho$
	$M_{\psi}^{(0)}$	$[\bar{c}\bar{c}(q\bar{q})_{I=0}]$	$I=0 \quad S=C=0$	$M_{\psi}^{(0)} \rightarrow \psi\eta; \psi\eta'; \psi\omega$
	$M_{\psi\psi}$	$(\bar{c}\bar{c}s\bar{s})$	$I=0 \quad S=C=0$	$M_{\psi\psi} \rightarrow \psi\psi; \psi K\bar{K}$
	H_{ψ}	$(\bar{c}\bar{c}g)$	$I=0 \quad S=C=0$	$H_{\psi} \rightarrow \psi\eta$
5. Similar states with hidden beauty	$M_{\psi}^{(1)}$	$[\bar{b}\bar{b}(q\bar{q})_{I=1}]$ etc.		$M_{\psi}^{(1)} \rightarrow \psi\eta$
6. Quasixotic baryons with hidden charm	R_{ψ}	$(qqq\bar{c})$	$I=3/2 \text{ and } I=1/2$	$R_{\psi} \rightarrow \psi N; A_c^0 D^0$
	$R_{\psi s}$	$(qqq\bar{c})$	$I=1 \text{ and } I=0$	$R_{\psi} \rightarrow \psi Y; A_c^0 D^0$
7. Similar baryons with hidden beauty	R_{ψ} etc.	$(qqq\bar{b})$		

Notes: Different decay channels for strange-charmed mesons, some which are given in the Table, are determined by the mass values of these particles: a) $M(P) > M(DK)$; b) $M(DK) > M(P) > M(D_s \pi)$; c) $M(D_s \pi) > M(P)$. For instance for P_c^0 mesons with $M(P_c^0) > M(D_s \pi)$ one may have only electromagnetic and weak decays, and for P_c^0 mesons with mass $M(P_c^0) < M(DK)$ only weak ones. Notations for mesons with open exotics: P_c - particles with "anomalous" strangeness; P_c - particles with "anomalous" isospin. The Table does not claim for completeness. Other exotic states with beauty and charmed quarks were also considered (see e.g., [26]).

COULOMB PRODUCTION OF HADRONS
AND STUDY OF HEAVY EXOTIC HADRONIC STATES

A2.1. General description of particle production
in the Coulomb field

In general the process of coherent production of "a" state by "h" on a nucleus with charge Z and atomic number A is fairly complex, since it originates from both electromagnetic and strong interactions (see diagrams of fig.26). The differential cross section coherent production of particle "a" on a nucleus has the form

$$d\sigma/dt|_c = |T_c + e^{i\varphi} T_s|^2, \quad (A2.1)$$

where T_c is the amplitude of Coulomb production, T_s is the amplitude of strong interaction (e.g. by the ω pole exchange), and φ is the relative phase of these amplitudes. In the approximation of the small-width resonance state "a" the electromagnetic cross section takes the form

$$\left. \frac{dt}{dt} \right|_c = |T_c|^2 \approx 8\pi\alpha Z^2 \frac{(2J_a+1)}{(2J_h+1)} \Gamma(a \rightarrow h\gamma) \left[\frac{m_a}{m_a^2 - m_h^2} \right]^3 \cdot \frac{|t-t_{\min}|}{s^2} |F_s(t)|^2. \quad (A2.2)$$

Here Z is the nucleus charge, α is the fine structure constant, $\Gamma(a \rightarrow h\gamma)$ is the radiative width of the corresponding decay "a", J_h and J_a are the spins of particles "h" and "a", m_h and m_a are their masses, $F_s(t)$ is the electromagnetic formfactor of the nucleus, $|t-t_{\min}| = (m_a^2 - m_h^2)^2 / 4P_h^2$ is the minimum value for the squared momentum transfer, P_h is the particle h momentum. If the primary particle is a photon then an additional factor of 2 enter the expression for the differential cross section.

The cross section of coherent production of a particle via a strong interaction mechanism is given by the expression

$$(d\sigma/dt|_s = |T_s|^2 = A^2 \cdot C_a |t-t_{\min}| \cdot |F_s(t)|^2.$$

Here A is the atomic number of the nucleus, C is a normalization factor for the "a" particle production on a single nucleon (this factor defines the contribution of the strong interaction mechanism), $F_g(t)$ is the hadronic formfactor of the nucleus (the formfactor $F_g(t)$ takes into consideration the corrections for rescattering and absorption of the primary and secondary particles in the nucleus).

As it follows from (A2.2) the cross section for the Coulomb production of a particle is proportional to the radiative decay width $\Gamma(a \rightarrow h\gamma)$. Therefore the measurement of the Coulomb process cross section makes it possible to find directly the absolute value for the radiative width. The difficulty lies in singling out the Coulomb process and suppressing the strong interactions background.

Fig.26 shows the general structure of the cross section of the Coulomb particle production. The Coulomb cross rises steeply with the decreasing momentum transfer. As is easily seen from (A.2.2) the cross section reaches its maximum at $|t_0| = 2|t_{\min}|$ and in this point $(d\sigma/dt)_c \propto |t_{\min}|^{-1} \propto P_h^2$. As the initial momentum increases, cross section at the maximum grows as P_h^2 , and the maximum itself shifts to smaller values of t . Here it occurs that the total value for the cross section of Coulomb particle production grows logarithmically with P_h . On the other hand, the cross section for a strong coherent process has a considerably wider t distribution, and, as a rule, it greatly decreases with the growth of incident energy (in the case ω exchange - as P_h^{-1}). Hence, with the growth of incident energy the effect of the Coulomb particle production becomes more distinct, and the strong interactions background rapidly vanishes.

A2.2. Search for Coulomb production of exotic hadrons

We shall consider electromagnetic production of exotic vector and isovector mesons with hidden strangeness $C(1480)^-$ as an example of applying the Coulomb mechanism for the study of the properties of exotic states

$$\pi^- + (Z, A) \rightarrow C(1480)^- + (Z, A). \quad (A2.4)$$

The neutral component of this isovector multiplet $C(1480) \rightarrow \phi\pi^0$ was observed with the LEPTON-P setup [21]. The discussions of the Coulomb mechanism in the search for exotic mesons, strongly

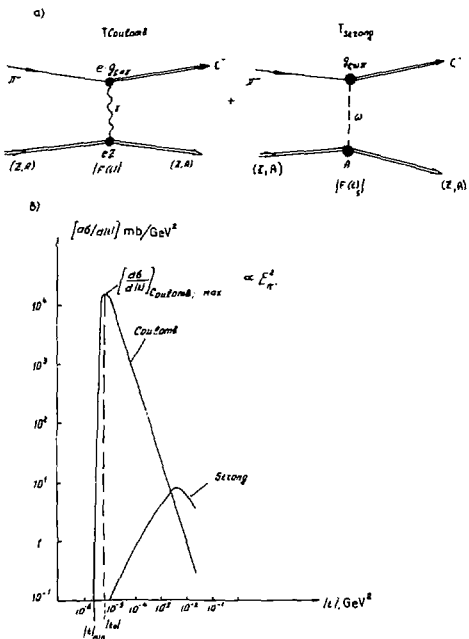


Fig. 26. Particle production in the nucleus Coulomb field: a) amplitude diagrams for coherent electromagnetic (T_{Coulomb}) and strong (T_{strong}) production of $C(1480)$ mesons by primary pions; b) general structure of the production cross section for the particles in coherent interactions with nuclei (see the text).

connected with the V_π channel may be found in [32]. As compared with hadronic process this precisely definite Coulomb mechanism allowed one to carry out more reliable the partial wave analysis and to single out new mesons, (see [32]).

The cross section for reaction (A2.2) turns out to be proportional to the radiative width $\Gamma[C(1480)^- \rightarrow \pi^- \gamma]$, which in the vector dominance model (VDM) has the form

$$\begin{aligned} \Gamma[C(1480)^- \rightarrow \pi^- \gamma] &= [\alpha / (g_\varphi^2 / \pi)] (K_\gamma / K_\varphi)^3 \Gamma[C(1480)^- \rightarrow \varphi \pi^-] = \\ &= [\alpha / (g_\varphi^2 / \pi)] (K_\gamma / K_\varphi)^3 \cdot \Gamma_c \cdot BR[C(1480)^- \rightarrow \pi^- \varphi] \approx \\ &\approx (7.4 \cdot 10^2 \text{ KeV}) \cdot BR[C(1480)^- \rightarrow \varphi \pi^-]. \end{aligned} \quad (A2.5)$$

Here K_γ , K_φ are photon and φ meson momenta for the corresponding decay channels of $C(1480)$ meson; $\Gamma_c = 130 \pm 60$ MeV its total decay width; $(g_\varphi^2 / \pi) \approx 9$ is the constant of the $\varphi \gamma$ transition in VDM^{*}.

Whereof and from (A2.2.) it follows

$$\begin{aligned} \sigma(C^- \rightarrow \pi \pi^-)_{\text{Coulomb}} &= \sigma[\pi^+ + (Z, A) \rightarrow C(1480)^- + (Z, A)] \cdot BR[C(1480)^- \rightarrow \pi \pi^-] \approx \\ &= 24\pi\alpha Z^2 \left[\frac{M_c}{M_c^2 - m_\pi^2} \right]^3 [BR(C(1480)^- \rightarrow \varphi \pi^-) \cdot \Gamma[C(1480) \rightarrow \pi^- \gamma] \times \\ &\times \int_{|t_{\min}|}^{\Delta} \left[\frac{|t - t_{\min}|}{t^2} \right] |F_Z(t)|^2 dt] \approx 24\pi\alpha Z^2 \left[\frac{M_c}{M_c^2 - m_\pi^2} \right]^3 \cdot [BR(C(1480)^- \rightarrow \varphi \pi^-)]^2 \times \\ &\approx (7.4 \cdot 10^2 \text{ KeV}) (\ln(\Delta / |t_{\min}|) - 1.51). \end{aligned} \quad (A2.6)$$

Here $|t_{\min}| = [M_c^2 - m_\pi^2]^2 / 4 F_\pi^2$; $\Delta \approx 1 \cdot 10^{-3} \text{ GeV}^2$ (for Pb nuclei); $F_Z(t)$ is the electromagnetic formfactor of the (Z, A) nucleus. For a lead target we have

^{*}The channel $C^- \rightarrow \omega \pi^-$; $\omega \rightarrow \gamma$ may also contribute to the width $\Gamma[C(1480)^- \rightarrow \pi^- \gamma]$. However for the exotic 4-quark C-meson with hidden strangeness this contribution seems to be small (besides $g_{\omega\pi}^{-2} = 1/2 g_\varphi^{-2}$).

$$\sigma(C^- \rightarrow \varphi\pi^-)_{\text{Coulomb}} \approx 2.5 \cdot 10^3 \mu\text{b} \cdot [\text{BR}(C(1480)^- \rightarrow \varphi\pi^-)]^2 \quad (\text{A2.7})$$

(at p_{π^-} equal to 1500 GeV).

The number of the events $N(C \rightarrow \varphi\pi^-)$ which can be

detected on the lead target with $4 \cdot 10^{21}$ Pb nuclei per cm^2 $\sim (1.4 \text{ g/cm}^2)$ in the π^- meson beam with the momentum $1.5 \cdot 10^3 \text{ GeV/c}$ per 10 days of the UNK accelerator operation (the detection efficiency being $\epsilon \approx 0.5$) is

$$N(C^- \rightarrow \varphi\pi^-) \approx 7.5 \cdot 10^6 [\text{BR}(C^- \rightarrow \varphi\pi^-)]^2. \quad (\text{A2.8})$$

If we assume that for the $C(1480)^- \rightarrow \varphi\pi^-$ identification $> 10^2$ events should be detected, then the sensitivity of this experiment will correspond to the branching ratio $\text{BR}(C^- \rightarrow \varphi\pi^-) < 4 \cdot 10^{-3}$. It should be stressed that the observation of $C(1480)^- \rightarrow \varphi\pi^-$ in the Coulomb production would allow one to unambiguously determine the partial branching $\text{BR}(C(1480)^- \rightarrow \varphi\pi^-)$, which is quite important for the interpretation of the nature of this hadron state [27].

The experiments on the hadron production by the Σ^- hyperon beam in the nucleus Coulomb field will also provide a solution for the problem of the existence of a narrow cryptoexotic baryon $\Sigma(3170)_{\varphi} = (qqss\bar{s})$ with $\Gamma(\Sigma_{\varphi}) < 20 \text{ MeV}$ observed in the reaction $K^- p \rightarrow \pi^- \Sigma(3170)_{\varphi}^+$ in several decay channels $\Sigma(3170)_{\varphi}^+ \rightarrow \Sigma K \bar{K} + n\pi$; $\Lambda K \bar{K} + n\pi$; $\Sigma K + n\pi$. The investigation of the mass spectrum for the final states on the coherent reactions of the type

$$\Sigma^- + \text{Pb} \rightarrow (\Sigma K \bar{K} + n\pi)^- + \text{Pb} \quad (\text{A2.10})$$

will allow one to search for $\Sigma(3170)$ baryons almost up to the cross sections $\sigma(\Sigma^- + \text{Pb} \rightarrow \Sigma(3170)_{\varphi}^- + \text{Pb}) \text{BR}$ (all detectable channels) $< 10^{-32} \text{ cm}^2/\text{nucleus}$.

For the value of $\text{BR} \sim 0.1$ the experiment sensitivity corresponds to the radiative width of $\Gamma[\Sigma(3170)_{\varphi}^- \rightarrow \Sigma^- \gamma] > 1 \text{ KeV}$. As it follows from VDM $\Gamma[\Sigma(3170)_{\varphi}^- \rightarrow \Sigma^- \gamma] \sim (\alpha / (g_{\varphi}^2 / \pi)) (K_{\gamma} / K_{\varphi})^2 \cdot \Gamma_{\Sigma_{\varphi}}$

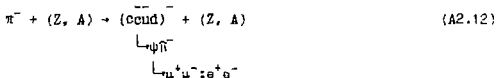
$BR(\Sigma_{\psi}^{-} \rightarrow \varphi \Sigma^{-})$. For $\Gamma_{\Sigma_{\psi}^{-}} \sim 20$ MeV $BR(\Sigma_{\psi}^{-} \rightarrow \varphi \Sigma^{-}) \sim 0.03$ correspond to the radiative width of 1 KeV.

In a more accurately detectable reaction

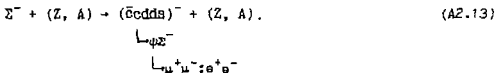


the sensitive of the experiment will correspond to $BR(\Sigma(3170)_{\psi}^{-} \rightarrow \varphi \Sigma^{-}) > 0.07$.

The Coulomb production of particles may also be used for the search of exotic and cryptoexotic mesons or baryons with hidden charm, e.g., in the reaction



or



Coherent production of heavy states requires very high energies, which may be available at the UNK only. Let us consider as an example reaction (A2.13) under assumption, that for the $\Sigma_{\psi}^{-} = (\bar{\text{c}}\text{udds})$ state the mass $m(\Sigma_{\psi}^{-}) \approx 5$ GeV and $\Gamma(\Sigma_{\psi}^{-}) \sim 150$ MeV.

Then by analogy with (A2.5) using VDM one may obtain the estimate

$$\Gamma(\Sigma_{\psi}^{-} \rightarrow \Sigma^{-} \gamma) = \{\alpha / (k_{\psi}^2 / \pi)\} (K_{\gamma} / K_{\psi})^2 \Gamma(\Sigma_{\psi}^{-} \rightarrow \Sigma^{-} \psi) \quad (\text{A2.14})$$

(for $(k_{\psi}^2 / \pi) \approx 10$, determined from the data on r ($\varphi \rightarrow e^{+} e^{-}$)).

In the same way as it was done earlier for (A2.4) and (A2.10) one can easily show that search for such $\Sigma(5000)_{\psi}$ baryons in reaction (A2.13) may be carried out with the sensitivity corresponding to $BR(\Sigma(5000)_{\psi} \rightarrow \Sigma^{-} \psi) > 0.07$.

SCINTILLATING FIBER VERTEX DETECTOR

Within the framework of our project on the construction of the vertex detector with scintillating fibers (SCIFI) we have studied the capillaries with liquid scintillator. Single component scintillator with local light emission based on methylnaphthalene with the scintillation efficiency 1.5 times higher than that of a standard polystyrene scintillator has been obtained. For the capillaries with the diameter of 30 μm the attenuation length $\lambda=50$ cm (starting from the capillary length of about 20 cm). In the absence of the light attenuation ~ 1 photoelectron is produced from each capillary. A unique quantum sensitivity of the image intensifier (II) (≈ 0.5), large light yield, high light trapping efficiency ($\approx 7\%$), good properties of glass cladding are among the advantages of the vertex detector.

The design of SCIFI with the diameter of $>25 \mu\text{m}$ and $\lambda=50$ cm considerably widens the range of applicability of this technique. It allowed to construct precise track detectors up to 1m or even a system of 10-20 cm coordinate planes going to one image intensifier.

A possibility to use a number of SCIFI planes with the readout by several charge coupling devices (CCD) as a track system for the vertex detector is being considered. In this case three MSD planes (out of four) in each of the first six stations of the vertex detector (fig.17) are replaced by three SCIFI planes. The sizes of the planes and deflection angle w.r.t. relative to beam is the same as for MSD. One MSD plane remains in front of each station to produce a trigger and improve time resolution of the SCIFI system. Each SCIFI plane is made of capillaries with the diameter 25 μm , and the plane is 1.5 mm thick along the beam. The light from the fibers is fed to three read out systems, each containing three IIs and one CCD (586x1088 cells with the dimensions $15 \times 15 \mu\text{m}^2$). Each image intensifier with amplification on a microchannel plate (MCP) is controlled by an external triggering signal. The image reduction

factor is $K=2.5$. $N=10$ photoelectrons are produced along the distance of $l=20$ cm in the plane 1.5 mm thick.

The coordinate resolution is determined by the fiber diameter and the number of photoelectrons on the track and it is equal to $\sigma=5 \mu\text{m}$. The two-track resolution is $\sim 50 \mu\text{m}$.

Readout system. The delay in the image intensifiers is about 100 ns, and the time of clearing the image in CCD is $1 \mu\text{s}$. Therefore this device requires a trigger of the first level (with the suppression of about 400 and the decision time of 100 ns), which allows to start recording the information from the vertex detector into the CCD. With the trigger of the next level the images are transferred into the memory section during $70 \mu\text{s}$ and is zipped by compressing the lines in such a way that the plane would occupy one line in the CCD. In the memory section up to 30 events can be buffered.

The resolution time is determined by the fluorescence decay time in first two IIs ($\tau \sim 80$ ns), in which the optical signal is delayed until a fast trigger is produced and the control signal is fed to the MCP of the last II. The resolution time is ~ 150 ns at control signal duration ~ 80 ns. The MSD planes improve the time resolution up to <10 ns. The optoelectronic delays which allow one to obtain the time resolution <10 ns have already been created.

The dead time (1ms) is equal to the time of the readout of an event when the frequency is $f=10$ MHz. At present there exists a CCD with $f>100$ MHz (the readout time is <0.1 ms).

The radiation resistance is determined by the type of the scintillator and is equal to $\sim 10^6$ rad, which is much better than that of semiconducting detectors, which may be used in the vertex detectors. When necessary the liquid scintillator is easily replaced.

The readout electronics of one CCD occupies <0.5 of the KAMAK (SUMMA) crate. All electronics for the fiber system occupies <1.5 of the crate.

When the number of tracks in an event is $n=25$ the information volume from 18 planes is 1.5 kbytes.

A considerably smaller amount of electronics, the price smaller by an order of magnitude and high radiation resistance are the advantages of the vertex detector with the scintillating

fibers as compared with the MSD version. If it is realized the number of the MSD registration channels may be greatly reduced (by 30-40%).

Appendix 4

VERTEX DETECTOR WITH CCD AND MSD

In this case the CCD is used as a detector, directly detecting charged particles. The vertex detector scheme is presented in fig.27. The vertex detector consists of 24 planes of microstrip silicon detectors and 8 planes of matrices based on the CCD : two joint CCD per one plane (16 CCD). The planes are alternated with the target matter. The matrices 458x580 cells $20 \times 20 \mu\text{m}^2$ will be used as CCDs. In a two-sectioned CCD the information from the accumulation section, installed in the beam and detecting the events, is transferred in the memory section and then is read out step by step. The cross section dimensions of the vertex detector are $0.9 \times 1.5 \text{ cm}^2$ (two accumulation sections of joint CCDs). The total number of the working cells in CCD is $2.1 \cdot 10^6$. The silicon substrate is $300 \mu\text{m}$ thick. The CCD ceramic support is outside the target. The longitudinal dimension of VD is 10 cm (0.05 nuclear length 0.1 radiative length). For our further calculation we chose the beam with the diameter of 5 mm and intensity $10^7/\text{s}$.

Each CCD plane is followed by three planes of microstrip detectors with a $50\text{-}100 \mu\text{m}$ step and characteristic dimensions $2 \times 2 \text{ cm}^2$, located at 90° and 45° respect each other. The strip detectors serve to work out a trigger, necessary for CCD control and additional coordinate indication as devices having better time resolution (10 ns).

The resolution time is determined by the differential smearing of the track at the moment of triggering signal arrival (until that moment CCD is switched off) and is equal to 400 ns ($T=300 \text{ K}$) or 100 ns ($T=100 \text{ K}$).

The dead time includes the time of transferring the information from the accumulation section to the memory section

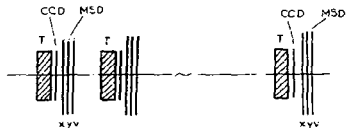


Fig. 27. The layout of the vertex detector with charge coupling devices and microstrip detectors: T - target, CCD - charge coupling devices, MSD - microstrip detectors.

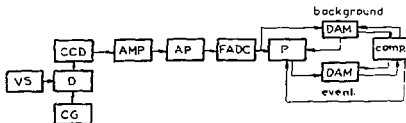


Fig. 28. Block-diagram for the readout electronics of the charge coupling devices: CG - control unit, VS - power supply, D - drivers, AMP - amplifier, AP - analog processor, FADC - flash analog-digital converter, P - processor of background subtraction and preliminary processing, DAM - fast memory, comp - computer.

(50 μ s) and readout time from the memory section (12.5 ms at $f=10$ MHz). All CCDs are read out in parallel. The CCDs with >100 MHz are being designed at present, and correspondingly the dead time will be reduced by an order of magnitude.

The maximum intensity acceptable for CCD is determined by the number of background particles during CCD sensitivity time. According to our estimates at the intensity of $10^7/s$ and beam halo of $10\% 3 \times 3$ cm² (0.5% per memory section) the number of the background cells will be <1300 ($<1\%$ of the area). Without halo the number of background cells will be <500 .

The pulse height is equal to $3 \cdot 5 \cdot 10^3$ electrons (potential well 10 μ m, diffusion collection from the depth of 30 ± 50 μ m) and with account of the diffusion smearing it will be equal to $1.5 \cdot 10^3$ per cell. The noise may be 50 ± 200 electrons depending on the temperature and readout frequency. The signal-to-noise ratio is 7 ± 30 .

The detection efficiency of single relativistic particle is $\sim 100\%$.

The CCD allows one to measure two coordinates in one plane with an accuracy 0.1 ± 6 μ m depending on the width of the charge distribution over the cells and on the noises. With $\sigma \sim 1$ μ m and 8 planes the vertex detector localizes the track with $\sigma_{xy}/8 = 0.4$ μ m.

The resolution between the tracks is <100 μ m without loss of accuracy.

The radiation resistance is $\sim 3 \cdot 10^5$ rad, which corresponds to the integral flux of $1.1 \cdot 10^{13}$ cm⁻². With the given geometry of the vertex detector this corresponds to 15 days of work at the flux of $\sim 4 \cdot 10^7$. Hence the problem of radiation resistance is connected with significant difficulties and should be studied more thoroughly. With an account of the CCD switch off up to the moment of the trigger arrival the radiation resistance might be improved by an order of magnitude.

The electronics circuit for CCD is presented in fig.28. It consists of a clock pulse generator, fixing the CCD working mode, computer-controlled supplies, drivers to work out control pulses for CCD, amplifiers ($K_{amp} \sim 200$), analog processors to suppress the noises with the frequency less than the readout frequency (10 MHz) and flash analog-to-digital converters to

digitize the signals (8 bits, 50 MHz), microprocessors for the pedestal level subtraction and selection of the useful clusters, fast memories to store the pedestal level (~130 kbyte/CCD) and events (~1 kbyte/event). The total amount of electronics for CCDs will occupy 5 crates. It will be possible to use special microprocessors for a joint operation of the microstrip detectors and CCDs and track coordinate reconstruction in the vertex detector.

Appendix 5

GENERAL BLOCK DIAGRAM OF DATA ACQUISITION

Main designations:

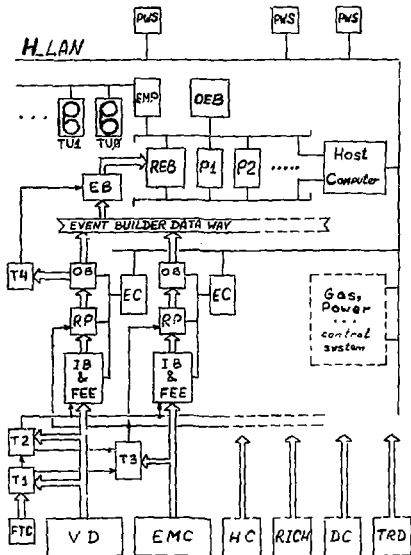
VD - vertex detector;
EMC - electromagnetic calorimeter;
HC - hadronic calorimeter;
RICH - Cerenkov ring image detector;
DC - minidrift chambers;
TRD - transition radiation detector;
FTC - flash trigger counters;
T1 - 1st level trigger system (over average $\langle E_{ATAR} \rangle$);
T2 - 2nd level trigger system (energy deposition jump ΔE);
T3 - 3d level trigger system ($E_T > E_{T cut}$);
T4-4th level trigger system (determination number of tracks and vertices in VD);
IB - output buffers of data acquisition system;
FEE - set of electron modules;
RP - data readout and compressing processor;
OB - output buffers of the low level of data acquisition system;
EB - Event Builder;
REB - row data buffer;
Fi - universal processors for event processing and final decision;
DEB - processed data buffer;
EMP-processor monitoring data flux and recording out the tape;

TU₁ - tape recorder;

Host computer;

PWS-working places for personal;

H-LAN - Hyperon Local Area Network.



Appendix 6

**COST OF THE MAIN EQUIPMENT FOR THE EXPERIMENTS
ON THE UNK HYPERON BEAM**

N	Item	Cost (mil. roubles)
1.	Tracking detectors (minidrift chambers; drift tubes ~35000 channels)	4.5
2.	Vertex detector (silicon microstrip detectors, charge coupling devices, scintillating fibre)	4.2
3.	RICH Cerenkov counters (3)	3.9
4.	Scintillation hodoscopes and detectors	1.1
5.	Cerenkov γ detectors of the GAME type (~3000 channels)	4.5
6.	Scintillation calorimeters (~10 ³ channels)	1.7
7.	Spectrometer magnets	4.5
8.	Cryogenic equipment	0.9
9.	Transition radiation detectors	3.1
10.	Metal structures, stands, measurement systems for magnetic fields, equipment for the control board and laboratories	3.8
11.	Electronics (detection and data acquisition system)	6.3
12.	Computers and their appliances	3.0
13.	Other expenditures	4.7
14.	Total cost	45.2 mil. roub. (for 12 mil. roub. for c.o.)
15.	Extra hard currency expenditures	0.83 mil. hard roub.

**On Sharing the Responsibilities Among the Participant
(IHEP, ITEP, LINP, INPS MSU)**

Sharing responsibilities among the Institutions:

1) IHEP - main contribution to Items 2 (CCD, scintillation fibre); 3; 5; 12 participation in 1; 4; 10; 11.

2) ITEP - main contribution to Items 6, 7, 8 participation in 1; 4; 5; 10; 11.

3) LINP - main contribution to 1, 2 (silicon detectors). 9; participation in 4; 10; 11.

4) INPS MSU - participation in 1, 3, 4, 5, 10, 11.

Approximate contribution of the Institutes to the construction of the facility

IHEP ~ 30%; ITEP ~ 30%; LINP 30%; INPS MSU ~ 10%.

This estimate is quite preliminary because of possible extension of collaboration.

REFERENCES

1. А.М.Зайцев, В.П.Кубаровский, Л.Г.Ландсберг и др.//
Материалы рабочего совещания "Физические исследования на УНК
ИФЭЭ", Протвино, 24-26 ноября 1981 г. с.90, Серпухов, 1982.
- А.А.Воробьев, Л.Г.Ландсберг, Е.М.Лейкинц и др. //Материалы
рабочего совещания по программе экспериментальных исследований
на УНК, Протвино, 14-19 сентября 1987 г., с.264, Серпухов, 1988.
- L.G.Landsberg.//Proc.of the International Europhysics Conference
on High Energy Physics, Uppsala, Sweden, June 25-July 1, 1987,
vol II, p.667.
2. В.И.Геркуш, В.П.Карташев, В.И.Котов и др. Препринт ИФЭЭ
88-188, Серпухов, 1988.
3. T.R.Cardello, P.S.Cooper, I.J.Teig et al. Preprint
FERMILAB-84/122E.
И.М.Беляев, И.А.Ветлицкий, М.В.Гришук и др. Препринт ИТЭФ N7-90,
Москва, 1990 г.
4. J.D.Bjorken. Preprint FERMILAB, 07/22/86.
5. W.H.Toki. Preprint SLAC-PUB-5094, Stanford, 1989
H.Nesemann, M.Reidenbach, W.Schmidt-Parzefall. Preprint
DESY-89-080, Hamburg, 1989.
6. N.S.Lockyer. //Proceedings of the Workshop on High Sensitivity
Beauty Physics at Fermilab, November 11-14, 1987, p.25.
7. B.Cox et al. //Fermilab Proposal 771, 1986.
8. B.Cox, D.Wagoner //Phys.of the Superconducting Supercollider,
p.83 Snowmass Co., 1986.
9. Proceedings of the Workshop on High Sensitivity Beauty Physics
at Fermilab, November 11-14, 1987.
10. T.Yoshida, M.R.Adams, C.N.Brown et al. //Phys.Rev. D, 1989,
vol.39, p.3516.
11. S.F.Bigli et al. //Phys. Lett.B, 1983, vol.122, p.456; 1985,
v.150, p.230; Z.Phys.C, 1985, vol.28, p.175.
12. P.Cetus, M.Binkley, F.Bossi et al. //Phys. Rev.Lett., 1987,
vol.59, p.1530.

13. S. J. Brodsky, J. F. Gunion. Preprint SLAC-PUB-3527, Stanford, 1984.
14. V. V. Kiselev, F. K. Likhoded, S. R. Slabospitsky. Preprint IHEP 86-45, Serpukhov, 1986.
15. S. S. Gershtein, V. V. Kiselev, A. K. Likhoded et al. Preprint IHEP 87-139, Serpukhov, 1987.
16. Я. И. Азимов, Н. Г. Уралцев, В. А. Хасе // ЯФ, 1987, т. 45, с. 1412.
17. R. D. Pesce // Материалы рабочего совещания по программе экспериментальных исследований на УНК, Протвино, 14-19 сентября 1987 г. с. 45, Серпухов, 1988.
18. B. Cox. Preprint FERMILAB-Conf.-88/33, Batavia, 1988.
19. P. Gilman. Preprint SLAC-PUB-4955, Stanford, 1989.
20. А. И. Алеев, В. А. Арефьев, В. П. Баладин и др. Препринт ОИЯИ Д-1-89-6146 Дубна 1989.
21. Л. Г. Ландсберг. // УФН, 1990, 160, вып. 3, с. 1.
22. "Glueballs, Hybrids and Exotic Hadrons" Upton. 1989.
23. H. J. Lipkin // Phys.Lett.B, 1977, vol.70, p.113.
N. Isgur, H. J. Lipkin // Phys.Lett.B, 1981, vol.99, p.151.
24. H. J. Lipkin // Phys.Lett.B, 1987, vol.195, p.484.
25. C. Gignoux, B. Silvestre-Brac, J. M. Richard // Phys.Lett., 1987, v.193, p.323.
26. М. И. Висоцкий, В. Д. Кекелидзе, А. Л. Леоимов и др. // Физические исследования на УНК ИФВЭ, Протвино 14-17 декабря 1982, с. 94, Серпухов, 1983.
27. Л. Г. Ландсберг. Препринт ИФВЭ 90-24, Серпухов, 1990.
28. M. Bourquin et al. // Phys.Lett.B, 1986, vol.172, p.113.
29. A. N. Aleev et al. // JINR Communications, M19-86, p.16, 1986.
Preprint JINR D1-88-368, Dubna, 1988; Preprint JINR D1-88-369, Dubna, 1988.
30. Hogaasen H., Sorba P. // Nucl.Phys.B, 1987, vol.145, p.269.
31. A. N. Aleev et al. // ЯФ, 1982, т. 36, с. 1420.
Z.Phys.C, 1984, vol.25, p.205.

32. M. Zielinski et al. //Z.Phys.C, 1986, vol.31, p.545.
M. Zielinski //Z.Phys.C, 1987, vol.34, p.255.
M. Zielinski // "Glueballs, Hybrids and Exotic Hadrons" Upton,
p.395.
33. Yu.D. Prokoshkin // Материалы рабочего совещания по программе
экспериментальных исследований на УИИ, Протвино, 14-19 сентября
1987 г. с.214. Серпухов, 1988.
34. M. Benayoun et al. //Nucl.Phys.B, 1987, vol.282, p.663.
35. С.С. Герштейн, Г.В. Джикия, А.А. Лахонел, Препринт ИИЭ 89-88
Серпухов, 1989.
36. S.D. Drell, T.-M. Yan //Phys.Rev.Lett, 1970, vol.25, p.316.
37. I.R. Kenyon //Rep.Prog.Phys., 1982, vol.42, p.1261.
R. Stroynowski //Phys.Rep., vol.71, p.1.
38. A.S. Ito et al. //Phys.Rev.D, 1981, vol.23, p.604.
39. S.R. Smith et al. //Phys.Rev.Lett, 1981, vol.46, p.1607.
40. J. Badier et al. //Z.Phys.C, 1983, vol.18, p.281; 1985, vol.26,
p.489.
41. B. Betev et al. //Z.Phys.C, 1985, vol.28, p.9; p.15.
42. D. Antreasyan et al. //Phys. Rev.Lett., 1982, vol.49, p.302.

Received 22 June, 1990.

CONTENTS

1. Introduction	23
2. UNK hyperon beam	25
3. Experimental facility for hyperon investigations	10
3.1. General structure of the setup	10
3.2. Simulation of the production and decay processes for baryons with heavy quarks.	12
4. Research program	19
4.1. Study of heavy quark physics.	19
4.1.1. Spectroscopy of strange-beauty and strange- charmed baryons.	24
4.1.2. Study of the mixing effects in the system of neutral B mesons.	28
4.1.3. Search for rare and forbidden heavy particle decays.	29
4.2. Search for heavy exotic hadrons.	30
4.3. Study of the Coulomb production of excited hyperon states (hyperon radiative widths).	38
4.4. Study of electromagnetic formfactors of unstable particles.	38
4.5. On measuring the Σ hyperon structure function.	42
4.6. Study of weak hyperon decays	46
5. Main elements of the experimental setup.	48
5.1. Hyperon beam identification system.	48
5.2. Vertex detector.	50
5.3. System of fiber track detectors	53
5.4. Track system	54
5.5. Secondary particle identification.	54
5.5.1. Ring image Cerenkov counters.	54
5.5.2. Transition radiation detectors	57
5.6. Triggering logics.	59
5.7. Data acquisition system	63
VI. General conclusions.	66
Appendix 1. Properties of heavy exotic states.	66
Appendix 2. Hadron Coulomb production and study of heavy exotic hadronic states.	68
Appendix 3. Vertex detector with scintillating fiber optics.	74

Appendix 4. Vertex detector with charge coupling devices	76
Appendix 5. General Block Diagram of Data Acquisition	79
Appendix 6. Cost of the main equipment for the experiments on the UNK hyperon beam.	81
References.	83

В.И.Геркуса и др.
Исследование на гммеронном пучке УИЯ.
Редактор А.А.Авдидова, Технический редактор Л.П.Тамасина.

Подписано к печати 4.VII.90. Т-11636. Формат 60x90/16.
Сфсетная печать. Печ.л. 5,15. Уч.-изд.л. 6,0. Тираж 270.
Заказ 1227. Индекс 3649. Цена 50 коп.

Институт физики высоких энергий, I42284, Протвино Москов-
ской обл.

90 коп.

Индекс 3649

ПРЕПРИНТ 90-81, ИФВЭ, 1990
